

PACO: Parts and Attributes of Common Objects

Vignesh Ramanathan*¹ Anmol Kalia*¹ Vladan Petrovic*¹ Yi Wen¹ Baixue Zheng¹
 Baishan Guo¹ Rui Wang¹ Aaron Marquez¹ Rama Kovvuri¹ Abhishek Kadian¹
 Amir Mousavi^{2†} Yiwen Song¹ Abhimanyu Dubey¹ Dhruv Mahajan¹
¹Meta AI ²Simon Fraser University

vigneshr@meta.com

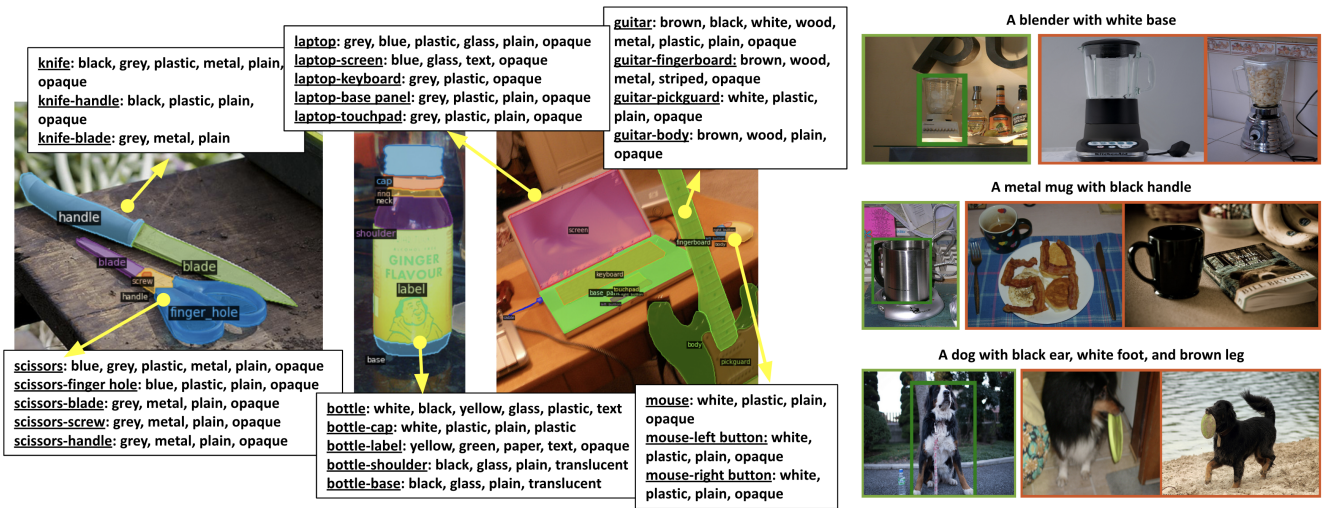


Figure 1. (left) PACO includes objects with object masks, object attributes, part masks, and part attributes. (right) Object instance queries composed of object and part attributes are shown with corresponding positive images in green and negative images in red.

Abstract

Object models are gradually progressing from predicting just category labels to providing detailed descriptions of object instances. This motivates the need for large datasets which go beyond traditional object masks and provide richer annotations such as part masks and attributes. Hence, we introduce PACO: Parts and Attributes of Common Objects. It spans 75 object categories, 456 object-part categories and 55 attributes across image (LVIS) and video (Ego4D) datasets. We provide 641K part masks annotated across 260K object boxes, with roughly half of them exhaustively annotated with attributes as well. We design evaluation metrics and provide benchmark results for three tasks on the dataset: part mask segmentation, object and part attribute prediction and zero-shot instance detection. Dataset, models, and code are open-sourced at <https://github.com/facebookresearch/paco>.

* Equal contribution † Work done during internship at Meta AI

1. Introduction

Today, tasks requiring fine-grained understanding of objects like open vocabulary detection [10, 16, 22, 55], GQA [19], and referring expressions [4, 23, 34] are gaining importance besides traditional object detection. Representing objects through category labels is no longer sufficient. A complete object description requires more fine-grained properties like object parts and their attributes, as shown by the queries in Fig. 1.

Currently, there are no large benchmark datasets for common objects with joint annotation of part masks, object attributes and part attributes (Fig. 1). Such datasets are found only in specific domains like clothing [20, 51], birds [45] and pedestrian description [27]. Current datasets with part masks for common objects [3, 17, 54] are limited in number of object instances with parts (59K for ADE20K [3] Tab. 1). On the attributes side, there exists large-scale datasets like Visual Genome [25], VAW [37] and

COCO-attributes [36] that provide object-level attributes. However, none have part-level attribute annotations.

In this work, we enable research for the joint task of object detection, part segmentation, and attribute recognition, by designing a new dataset: PACO. With video object description becoming more widely studied as well [21], we construct both an image dataset (sourced from LVIS [15]) and a video dataset (sourced from Ego4D [13]) as part of PACO. Overall, PACO has 641K part masks annotated in 77K images for 260K object instances across 75 object classes and 456 object-specific part classes. It has an order of magnitude more objects with parts, compared to recently introduced PartImageNet dataset [17]. PACO further provides annotations for 55 different attributes for both objects and parts. We conducted user studies and multi-round manual curation to identify high-quality vocabulary of parts and attributes.

Along with the dataset, we provide three associated benchmark tasks to help the community evaluate its progress over time. These tasks include: a) part segmentation, b) attribute detection for objects and object-parts and c) zero-shot instance detection with part/attribute queries. The first two tasks are aimed at benchmarking stand alone capabilities of part and attribute understanding. The third task evaluates models directly for a downstream task.

While building the dataset and benchmarks, we navigate some key design choices: (a) Should we evaluate parts and attributes conditioned on the object or independent of the objects (eg: evaluating “leg” vs. “dog-leg”, “red” vs. “red cup”)? (b) How do we keep annotation workload limited without compromising fair benchmarking?

To answer the first question, we observed that the same semantic part can visually manifest very differently in different objects (“dog-leg” vs “chair-leg”). This makes the parts of different objects virtually independent classes, prompting us to evaluate them separately. This also forces models to not just identify parts or attributes independently, but predict objects, parts and attributes jointly. This is more useful for downstream applications.

Next, to keep annotation costs limited, we can construct a federated dataset as suggested in LVIS [15]. For object detection, LVIS showed that this enables fair evaluation without needing exhaustive annotations for every image. However, this poses a specific challenge in our setup. Object detection requires every region to be associated with only one label (object category), while we require multiple labels: object, part and attribute jointly. This subtle but important difference, makes it non-trivial to extend definition and implementation of metrics from LVIS to our setup. We provide a nuanced treatment of missing labels at different levels (missing attribute labels vs. missing part and attribute labels) to handle this.

Our design choices allow us to use popular detection

metrics: Average Precision and Average Recall for all our tasks. To facilitate calibration of future research models, we also provide benchmark numbers for all tasks using simple variants of mask R-CNN [18] and ViT-det [30]. Dataset, models, and code are open-sourced at <https://github.com/facebookresearch/paco>.

1.1. Related work

Availability of large-scale datasets like ImageNet [5], COCO [32], LVIS [15] have played a crucial role in the acceleration of object understanding. We briefly review datasets that provide a variety of annotations for objects besides category labels.

Object detection and segmentation datasets

The task of detecting and segmenting object instances is well studied with popular benchmark datasets such as COCO [32], LVIS [15], Object365 [40], Open Images [26] and Pascal [9] for common objects. There are also domain-specific datasets for fashion [20, 51], medical images [49] and OCR [7, 42, 44]. Recent datasets like LVIS, Open Images and Objects365 have focused on building larger object-level vocabulary without specific focus on parts or attributes. In particular, LVIS introduced the idea of federated annotations, making it possible to scale to larger vocabularies without drastically increasing annotation costs. We adopt this in our dataset construction as well.

Part datasets

Pixel-level part annotations for common objects are provided by multiple datasets such as PartImageNet [17], PASCAL-Part [3], ADE20K [53, 54] and Cityscapes-Panoptic-Parts [35]. PASCAL provides part annotations for 20 object classes and PartImageNet provides parts for animals, vehicles and bottle. Cityscapes has parts defined for 9 object classes. In contrast we focus on a larger set of 75 common objects from LVIS vocabulary. Our dataset has ten times larger number of object boxes annotated with part masks compared to PartImageNet. ADE20K is a 28K image dataset for scene parsing which includes part masks. While it provides an instance segmentation benchmark for 100 object categories, part segmentation is benchmarked only for 8 object categories due to limited annotations. We provide a part segmentation benchmark for all 75 object classes. More detailed comparison of above datasets are provided in Tab. 1. Apart from common objects, part segmentation has also been studied for specific domains like human part segmentation: LIP [12], CIHP [50], MHP [28], birds: CUB-200 [45], fashion: ModaNet [51], Fashionpedia and cars: CarFusion [8], ApolloCar3D [43].

Attribute datasets

Attributes have long been viewed as a fundamental way to describe objects. In particular, domain-specific attribute datasets have become more prevalent for fashion, animals, people, faces and scenes [14, 24, 29, 33, 52, 54]. A motivation

	PartsIN	Pascal	City.-PP	VAW	COCO att.	FashionPedia	ADE	PACO-LVIS	PACO-EGO4D	PACO
object domain	comm.	comm.	comm.	comm.	comm.	fashion	comm.	comm.	comm.	comm.
# obj cats	158	20	5	2260	29	27	2693	75	75	75
# img with obj mask	24K	20K	3.5K	72.3K	84K	48.8K	27.6K	57.6K	23.9K	81.5K
# obj mask	24K	50k	56k	260.9K	180K	167.7K	434.8K	274K	58.4K	332.3K
# obj-part cats	609	193	23	-	-	-	476	456	456	456
# obj-agn. part cats	13	127	9	-	-	19	-	200	194	200
# img with part mask	24K	19K	3.5K	-	-	48.8K	12.6K	52.7K	24K	76.7K
# part mask	112K	363.5k	100k	-	-	174.4K	193.2K	502K	139.3K	641.4K
# obj with part mask	24K	40k	31k	-	-	NA	59K	209.4K	50.9K	260.3K
# att cats	-	-	-	620	196	294	1314	55	55	55
# img with att	-	-	-	72.3K	84K	48.8K	16.3K	48.6K	26.3K	74.9K
# obj with att	-	-	-	260.9K	180K	78.9K	74.6K	74.4K	49.6K	124K
# part with att	-	-	-	-	-	132.8K	31.4K	186K	110.6K	296.6K
avg # att / img	-	-	-	3.6	41	8.4	24.7	22.2	25.8	23.4
neg. att labels	-	-	-	TRUE	TRUE	TRUE	FALSE	TRUE	TRUE	TRUE

Table 1. Comparison of publicly available parts and attributes datasets. PartsIN refers to PartsImageNet, City.-PP refers to Cityscape PanopticParts. Salient features of our dataset are shown in bold.

of our work is to extend such rich descriptions to common objects and object parts as well. More recently, Pham et al. [37] introduced the Visual Attributes in the Wild (VAW) dataset constructed from two source datasets: VGPhrase-Cut [46] and GQA [19]. VAW expanded and cleaned the attributes in the source datasets, and adds explicit negative attribute annotations to provide a rigorous benchmark for object attribute classification. VAW solely focused on attribute classification, and assumed the object box and label to be known apriori. VAW is not benchmarked for joint end-to-end object/part localization and attribute recognition, which is the focus of our work.

Part and attribute datasets

Fashionpedia [20] is a popular dataset for fashion providing both part and attribute annotations in an image. It is the closest line of work that also provides part localization and attribute recognition benchmarks. PACO aims to generalize this to common object categories.

Instance recognition with queries

Attributes have been long used for zero-shot object recognition [39, 48]. We use this observation to build an instance-level retrieval benchmark for retrieving a specific instance of an object from a collection of images using part and attribute queries. Recently, Cops-Ref [4] also introduced a challenging benchmark for object retrieval in the natural language setting with a focus on referring expressions [23, 34] that involve spatial relationships between objects. PACO is aimed at benchmarking part and attribute based queries at varying levels of compositions.

2. Dataset construction

2.1. Image sources

PACO is constructed from LVIS [15] in the image domain and Ego4D [13] in the video domain. We chose LVIS due to its large object vocabulary and federated dataset con-

struction. Ego4D has temporally aligned narrations, making it easy to source frames corresponding to specific objects.

2.2. Object vocabulary selection

We first mined all object categories mentioned in the narrations accompanying Ego4D and took the intersection with common and frequent categories in LVIS. We then chose categories with at-least 20 instances in Ego4D, resulting in 75 categories commonly found in both LVIS and Ego4D.

2.3. Parts vocabulary selection

Excluding specific domains like fashion [20], there is no exhaustive ontology of parts for common objects. We mined part names from web-images obtained through queries like “parts of a car”. These images list part-names along with illustrations and pointers to the parts in the object. We manually curate such mined part names for an object category to only retain parts that are visible in majority of the object instances and clearly distinguishable. More details in the appendix. This resulted in a total of 200 part classes shared across all 75 objects. When expanded to object-specific parts this results in 456 object-part classes.

2.4. Attribute vocabulary selection

Attributes are particularly useful in distinguishing different instances of the same object type. Motivated by this, we conducted an in-depth user study (details in appendix) to identify the sufficient set of attributes that can separate all object instances in our dataset. This led to the final vocabulary of 29 colors, 10 patterns and markings, 13 materials and 3 levels of reflectance.

2.5. Annotation pipeline

Our overall data annotation pipeline consists of: a) Object bounding box and mask annotation (only for Ego4D)

b) part mask annotation, c) object and part attributes annotation and d) instance IDs annotation (only for Ego4D).

2.5.1 Object annotation

Bounding boxes and masks are already available for the 75 object classes in LVIS, but not in Ego4D. For Ego4D, we use the provided narrations to identify timestamps in videos for specific object classes. We sampled 100 frames around these timestamps and asked annotators to choose at most 5 diverse (in lighting, viewpoint, etc.) frames that depict an instance of the object class. These frames are annotated with bounding boxes and object masks. A frame annotated with a specific object class is exhaustively annotated with every bounding box of the object class. For each object class in the evaluation splits we annotate negative images that are guaranteed to not contain the object.

2.5.2 Part mask annotation

We provide part masks for all annotated object boxes in both LVIS and Ego4D. A fraction of the object boxes were rejected by annotators due to low resolution, motion blur or significant occlusion. This resulted in a total of 209K, 43K object boxes with parts in LVIS, Ego4D respectively. For an object box to be annotated, we listed all the potential parts for the object class and asked annotators to annotate masks for the visible parts. Note that parts can be overlapping (for example, door and handle). We do not distinguish between different instances of a part in an object instance, but provide a single mask covering all pixels of a part class in the object (e.g., all car wheels are covered by a single mask).

2.5.3 Attributes annotation

Every bounding box in Ego4D is annotated with object and part-level attributes, unless rejected by annotators due to lack of resolution or blur. Obtaining exhaustive attribute annotations for all object and part instances in LVIS dataset for the 75 categories is very expensive. Hence, we randomly selected one medium or large¹ bounding box per image, per object class for attribute annotations. We annotate a box with both object-level and part-level attributes for all 55 attributes in a single annotation job. This ensures consistency between object and part attributes and helped us annotate attributes for a diverse set of images with limited expense. This resulted in 74K (50K) object instances and 186K (111K) part instances annotated with attributes for LVIS (Ego4D) respectively.

¹Decided based on box area as defined in COCO [44].

2.5.4 Instance annotation

We also introduce a zero-shot instance detection task with our dataset. To do this we need unique instance IDs for each object box in the dataset. For LVIS data, we assume each individual object box to be a separate instance. However, this is not true for Ego4D. Different bounding boxes of an object could correspond to the same instance. Also, different videos in Ego4D could have the same object instance. We underwent a rigorous multi-stage process to annotate instance IDs, explained in the appendix. This resulted in 16908 unique object instances among the 49955 annotated object boxes in Ego4D.

2.5.5 Managing annotation quality

Each stage in the annotation pipeline had multiple associated quality control methods such as use of gold standard and annotation audits. We had 10 – 50 instances of each object annotated by expert annotators and set aside as gold annotations. For part mask annotations, we measured mIoU with gold images for each object class and re-annotated object classes with mIoU < 50% on gold annotations. Eventually, 90% of the object classes have mIoU ≥ 0.75 with the gold-annotated masks (shown in appendix). For all attribute annotations we were checking quality by randomly sampling annotations, finding patterns in annotation errors, updating guidelines to correct clear biases, and re-annotating erroneous examples. This eventually drove accuracy to more than 85% on the gold annotations provided by expert annotators.

3. Dataset statistics

Part statistics: Fig. 2a shows the number of part masks annotated for each object-part category in PACO-LVIS and PACO-EGO4D. We observe the typical long-tail distribution with certain categories like ‘book-cover’, ‘chair-back’ and ‘box-side’ having greater than 6500 instances, and, categories like ‘fan-logo’ and ‘kettle-cable’ having fewer than 5 instances. Fig. 2b shows the distribution of number of large, medium and small parts in PACO-LVIS. We observe that larger fraction of part masks belong to low and medium size, compared to object masks.

Attribute statistics: Fig. 2c shows number of annotations per attribute and attribute type in PACO-LVIS. We again observe a long-tail distribution with common attributes like colors having many annotations, while uncommon ones like ‘translucent’ having fewer annotations.

Comparison with other datasets: We also provide an overview of different parts and/or attributes datasets in Tab. 1. Among the datasets with part annotations, PACO provides 641K part mask annotations in the joint dataset, which is $3\times$ bigger than other datasets like ADE20K

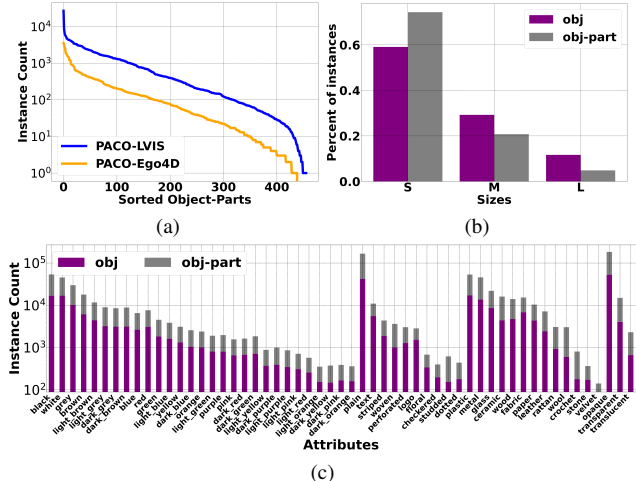


Figure 2. Dataset Statistics. Fig. (a) shows the distribution of instances across the 456 object-part categories. Fig. (b) shows the size distribution of object and part masks in PACO-LVIS. Fig. (c) shows the distribution of the 55 attribute classes across instances in PACO-LVIS

(176K), PartImageNet (112K) and Fashionpedia (175K). While ADE20K has sizeable number of part masks overall, it doesn't provide a well defined instance-level benchmark for parts due to limited test annotations. PACO has 10 \times more object instances with parts (260K) compared to the next closest parts benchmark dataset for common objects: PartsImageNet (25K). In terms of attributes, the joint dataset has 124K object and 297K part masks with attribute annotations. While VAW has 261K object masks with attributes, the combined set of attribute annotations for part and object masks (421K) in PACO is still larger. VAW has a larger vocabulary of attributes 620 vs 55. However, in PACO, every object/part mask annotated with attributes is exhaustively annotated with all attributes in the vocabulary unlike VAW. This makes the density of attributes per image 23.4 much larger than VAW 3.6. COCO-attributes provides attribute annotations for COCO images as well, but for much smaller set of object classes (29).

4. Tasks and evaluation benchmark

We now introduce three evaluation tasks. Our first two tasks directly evaluate the quality of parts segmentation and attributes prediction. The other task aims to leverage parts and attributes for zero-shot object instance detection.

4.1. Dataset splits

We split both PACO-LVIS and PACO-EGO4D datasets into `train`, `val` and `test` sets. The `test` split of PACO-LVIS is a strict subset of the LVIS-v1 `val` split and contains 9443 images. The `train` and `val` splits of PACO-

LVIS are obtained by randomly splitting LVIS-v1 `train` subset for 75 classes, and contain 45790 and 2410 images respectively. Ego4D is split into 15667 `train`, 825 `val` and 9892 `test` images. The set of object instance IDs in Ego4D `train` and `test` sets are disjoint.

4.2. Federated dataset for object categories

We briefly review the concept of federated dataset from LVIS [15], where every image in the evaluation set is not annotated exhaustively with all object categories. However, every object category has (a) a set of *negative images* that are guaranteed to not contain any instance of the object, (b) a set of *exhaustive positive images* where all instances of the object are annotated and (c) a set of *non-exhaustive positive images* with at-least one instance of the object annotated. Non-exhaustive positive images are not guaranteed to have all instances of the object annotated. Only these three types of images are used to evaluate AP for the category.

4.3. Part segmentation

Our part segmentation task requires an algorithm to detect and segment the part-masks of different object instances in an unseen image and assign an $(object, part)$ label with a confidence score to the part-mask. The $(object, part)$ pairs are from a fixed know set. This is similar to the object instance segmentation task, but uses object-part labels instead of only object labels. We consider parts of different instances of the object in an image to be different object-part instances.

We choose to evaluate the task for $(object, part)$ labels instead of only *part* labels, since the appearance and definition of the same semantic part can be very different depending on the object it appears in. We expect the models to produce both an object and a part label, with a single joint score. This leaves us with 456² object-parts in the dataset.

We use mask and box Average Precision (AP) metrics defined in COCO [44]. AP is averaged over different thresholds of intersection over union (IoU)³.

AP calculation in federated setup

Given a set of predicted masks with a combined score for (object category o , part category p), we compute AP for the object-part (o, p) at a given IoU threshold. We use all positive and negative images of o to do this. We treat each predicted mask as a *true positive*, *false positive* or *ignore* it based on the following criteria.

Negative images: We treat all predicted masks in negative images of object o as *false positives* for the object-part (o, p) . This is a valid choice, since an object-part cannot be present without the object.

²Similar to LVIS, a small number of valid $(object, part)$ pairs in `train` do not have any annotated instances in the `val` and `test` splits. We ignore these object-parts for evaluation.

³Mask IoU is used for mask AP and box IoU is used for box AP [44]

Model	mask AP		box AP	
	AP^{obj}	AP^{opart}	AP^{obj}	AP^{opart}
R50 FPN	31.5 ± 0.3	12.3 ± 0.1	34.6 ± 0.3	16.0 ± 0.1
+ cascade	32.6 ± 1.3	12.5 ± 0.7	37.4 ± 1.6	16.3 ± 1.1
R101 FPN	31.5 ± 0.6	12.3 ± 0.3	34.8 ± 0.8	16.1 ± 0.3
+ cascade	35.1 ± 0.1	13.7 ± 0.1	40.2 ± 0.1	17.9 ± 0.2
ViT-B FPN	33.6 ± 0.3	13.5 ± 0.1	38.7 ± 0.4	17.5 ± 0.0
+ cascade	33.6 ± 0.3	13.5 ± 0.1	38.7 ± 0.4	17.5 ± 0.0
ViT-L FPN	42.8 ± 0.3	17.3 ± 0.1	47.3 ± 0.2	22.0 ± 0.1
+ cascade	43.4 ± 0.3	17.7 ± 0.0	49.7 ± 0.2	22.9 ± 0.0

Table 2. Object and object-part segmentation results for mask-RCNN and ViT-det models trained and evaluated on PACO-LVIS

Non-exhaustive positive images: We treat images marked as non-exhaustive for the object category as non-exhaustive for the object-part as well. There is also a subset of images exhaustively annotated for the object, but not for the object-part. We provide an explicit flag to identify such additional non-exhaustive images for every object-part in our datasets. In both cases of non-exhaustive images, we consider predicted masks overlapping (above the IoU threshold) with an annotated ground-truth object-part mask as *true positives*. We *ignore* other predicted masks in the images.

Exhaustive positive images: On the subset of positive images, where every instance of the object-part is exhaustively annotated, we treat predicted masks as *true positives* if they overlap (above the threshold) with a ground-truth annotated part mask, otherwise they are treated as *false positives*.

The true and false positive masks along with their predicted scores are used to calculate AP at a given threshold as defined in COCO [44]. We report mean Average Precision across all object-part categories (AP^{opart}).

4.4. Instance-level attributes prediction

In PACO, this is the task that requires an algorithm to produce masks and/or boxes along with both a category label (object or object-part) as well as an attribute label and a single joint confidence score for the category with the attribute (eg.: score for “red car”, “red car-wheel”).

Since multiple aspects are being evaluated together, we need to be meticulous in designing the evaluation metric. In particular, we need to be careful in our consideration of object and object-part masks with missing attribute annotations as we show next.

AP calculation in federated setup

We continue with AP as our evaluation metric. Given a set of predicted masks with scores for a category c (can be an object o or object-part (o, p)) and attribute a combination, we compute AP for (c, a) . We use all positive or negative images of object o to compute the AP for (c, a) . We compute AP at different IoU thresholds and report the average. At a given threshold, we identify true positives, false positives or ignored masks as described below.

Negative images: We treat all predicted masks in negative images of the object o as *false positives* for (c, a) .

Positive images: In both exhaustive and non-exhaustive positive images, we do the following. We treat masks overlapping with ground-truth masks of the category that are also annotated positively for the attribute a as *true positives*. Masks overlapping with ground truth masks of the category c , but annotated negatively for attribute a are treated as *false positives*. We *ignore* mask predictions that overlap with ground-truth masks of category c with un-annotated attribute labels. We differ in the treatment of mask predictions not overlapping with any ground-truth mask of the category, in exhaustive and non-exhaustive positive images. In case of non-exhaustive images, we *ignore* such predictions, while in exhaustive images we treat such predictions as *false positives*.

We use the true and false positives along with their predicted confidence scores to calculate AP for (c, a) . We only compute AP for (c, a) if at-least one instance of c is positively annotated with attribute a in test set and at-least 40 other instances of c are negatively annotated for a .

We observe that some (c, a) combinations can be “rare” in the evaluation set with few positive occurrences only. As observed in LVIS [15] such “rare” combinations can have a higher variance in the metric and it helps to average the metric across categories to reduce variance. Hence, we aggregate AP at an attribute level for a , by averaging the AP across all categories that are evaluated with a . We aggregate over object categories and object-part categories separately, leading to object AP (AP_a^{obj}) and object-part AP (AP_a^{opart}) for each attribute a . In our experiments, we report the mean value of AP_a^{obj} across all attributes: AP_{att}^{obj} , as well as the mean values across attributes belonging to color (AP_{col}^{obj}), pattern & markings (AP_{pat}^{obj}), material (AP_{mat}^{obj}) and reflectance (AP_{ref}^{obj}). We do the same for object-parts and report AP_{att}^{opart} , AP_{col}^{opart} , AP_{pat}^{opart} , AP_{mat}^{opart} and AP_{ref}^{opart} .

4.5. Zero-shot instance detection

Zero-shot instance detection requires an algorithm to retrieve the bounding box of a specific instance of an object based on a “query” describing the instance. No sample images of the instance are previously seen by the algorithm. This has similarity to referring expression tasks [4, 23, 34] that localize a specific object instance in an image based on attribute and spatial relation queries. However, we introduce a more fine-grained evaluation benchmark, where the queries are composed of both object and part attributes at different levels of composition.

We construct the evaluation dataset for both LVIS and Ego4D from their corresponding test splits. We first define level- k (Lk) query as describing an object instance in terms of k attributes of the object and/or parts. For exam-

Model	AP_{att}^{obj}	AP_{col}^{obj}	AP_{pat}^{obj}	AP_{mat}^{obj}	AP_{ref}^{obj}	AP_{att}^{opart}	AP_{col}^{opart}	AP_{pat}^{opart}	AP_{mat}^{opart}	AP_{ref}^{opart}
R50 FPN	13.5 ± 0.3	10.8 ± 0.1	14.1 ± 0.6	9.9 ± 0.4	19.1 ± 0.7	9.7 ± 0.2	10.7 ± 0.2	10.6 ± 0.5	6.9 ± 0.0	10.7 ± 0.2
+ cascade	15.0 ± 1.0	12.4 ± 0.7	16.1 ± 0.7	11.0 ± 0.9	20.6 ± 1.6	10.5 ± 0.7	11.6 ± 0.8	11.6 ± 0.8	7.6 ± 0.7	11.2 ± 0.7
R101 FPN	13.5 ± 0.3	11.0 ± 0.2	13.9 ± 0.3	9.9 ± 0.4	19.1 ± 0.6	9.9 ± 0.1	11.0 ± 0.4	10.8 ± 0.4	7.1 ± 0.2	10.9 ± 0.3
+ cascade	16.0 ± 0.1	13.4 ± 0.2	16.7 ± 0.2	12.3 ± 0.1	21.5 ± 0.4	11.5 ± 0.2	12.6 ± 0.1	12.5 ± 0.3	8.5 ± 0.3	12.6 ± 0.3
ViT-B FPN	15.0 ± 0.2	11.9 ± 0.1	14.9 ± 0.5	12.8 ± 0.4	20.4 ± 0.8	10.9 ± 0.2	11.3 ± 0.3	11.4 ± 0.6	9.0 ± 0.1	11.8 ± 0.3
+ cascade	15.7 ± 0.2	12.6 ± 0.1	16.0 ± 0.5	13.2 ± 0.4	20.9 ± 0.5	11.0 ± 0.2	11.6 ± 0.2	11.7 ± 0.4	9.0 ± 0.2	11.5 ± 0.3
ViT-L FPN	18.8 ± 0.3	14.9 ± 0.2	18.9 ± 1.0	16.0 ± 0.7	25.4 ± 0.7	13.5 ± 0.2	14.0 ± 0.2	14.0 ± 0.4	11.7 ± 0.4	14.3 ± 0.6
+ cascade	19.5 ± 0.3	15.6 ± 0.3	19.1 ± 0.5	16.3 ± 0.3	27.0 ± 0.4	13.8 ± 0.1	14.4 ± 0.3	15.1 ± 0.0	11.5 ± 0.2	14.5 ± 0.4

Table 3. Attribute prediction results for mask R-CNN and ViT-det models trained and evaluated on PACO-LVIS. Box AP results are shown for both object attributes and object-part attributes prediction.

Model	LB-no attribute	Original	UB-perfect attribute
R-50 FPN	8.6 ± 0.3	13.5 ± 0.3	61.4 ± 0.3
R-101 FPN	8.6 ± 0.3	13.5 ± 0.3	63.0 ± 0.3
ViT-B FPN	9.0 ± 0.1	15.0 ± 0.2	60.5 ± 0.1
ViT-L FPN	10.6 ± 0.2	18.8 ± 0.3	72.6 ± 0.3

Table 4. Bounds for AP_{att}^{obj} keeping detection quality fixed and changing attribute scores. For lower bound (LB), we neglect attribute scores and for upper bound (UB), we assume perfect attribute scores.

ple, "blue mug" or "mug with a blue handle" are sample L1 queries, "blue striped mug" is a L2 query and "blue striped mug with white handle" is a L3 query. Each query is associated with 1 positive image with a bounding box and a distractor set of up to 100 images, see Fig 1.

To ensure practical utility, we avoid queries with uninformative attributes like "car with a black wheel" since all cars have black wheel and eliminate part names that are infrequently used in large multimodal datasets (PMD [41]). The distractor images for each query contain hard-negatives corresponding to other instances of the same object category, but differing by at-least one attribute from the query. Queries have more than 40% hard negatives on average. PACO-LVIS has 931/2348/2000 and PACO-EGO4D has 793/1437/2115 L1/L2/L3 queries respectively.

We measure performance of an algorithm through average recall metrics $AR@k$ where $k = 1, 5$ denotes the top- k boxes returned by the method for a query. We compute AR at different IoU thresholds and report the average over all thresholds, as defined in COCO [44].

5. Benchmarking experiments

5.1. Part segmentation

We train two mask R-CNN and two ViT-det [30] models with 531 classes comprising both 75 object categories and 456 object-part categories. We use the standard 100-epoch schedule recommended for LVIS with federated loss [56] and LSJ [11] augmentation. For all experiments on part segmentation and attribute detection, we train on `train`, search for hyper-parameters on `val` and report results on `test` splits. More implementation details are in the ap-

pendix. We trained with Cascade [1] as well as Feature Pyramid Network (FPN) [31]. The results for models trained and evaluated on PACO-LVIS are summarized in Tab. 2. We also provide results for models trained on joint image + video PACO dataset in the appendix.

We observed that object-parts in general have a smaller AP compared to objects. This is due to the typically smaller size of parts compared to objects (Fig. 2b). Nevertheless larger and better backbones like ViT-L are seen to improve performance for the part segmentation task.

5.2. Instance-level attributes prediction

We train a simple extensions of mask R-CNN and ViT-det models with an additional attribute head on the shared backbone. The attribute head uses the same ROI-pooled features as the detection head to predict object and object-part attributes. We use a separate cross-entropy loss for each attribute type. The model is shown in more detail in the appendix. We report box AP values for models trained on PACO-LVIS in Tab. 3. We also provide results for the joint dataset in the appendix. During inference, we rank the detected boxes for a specific object-attribute combination by the product of the corresponding object and attribute scores. For parts, we rank boxes by product of corresponding object-part score and attribute score.

Attribute prediction is a much harder task than object detection, as witnessed by the lower AP values for both object-attributes and object-part-attributes, compared to object and part AP in Tab. 2. We observe larger models fairing better for this task as well.

Since we measure multiple factors together, we analyze the sensitivity of AP_{attr}^{obj} only to attribute prediction in Tab. 4. To do so, we keep detections from the trained models fixed and get (a) lower bounds by ignoring attribute scores and (b) upper bounds by assuming perfect attribute scores (details in appendix). We observe a huge gap between lower and upper bounds, with our original models only partially bridging it. This shows scope for future improvements in the attribute prediction ability of the models.

Model	L1 queries		L2 queries		L3 queries		all queries	
	AR@1	AR@5	AR@1	AR@5	AR@1	AR@5	AR@1	AR@5
R50 FPN	22.5 ± 0.7	39.2 ± 0.5	20.1 ± 0.4	38.5 ± 0.1	22.3 ± 0.9	44.5 ± 1.1	21.4 ± 0.6	40.9 ± 0.3
R101 FPN	23.1 ± 0.7	40.5 ± 1.4	20.0 ± 0.6	39.3 ± 1.0	23.1 ± 0.7	45.2 ± 0.6	21.7 ± 0.6	41.8 ± 0.8
ViT-B FPN	26.8 ± 0.2	45.8 ± 0.2	22.7 ± 0.5	40.0 ± 0.7	24.1 ± 0.5	42.5 ± 1.5	23.9 ± 0.4	42.0 ± 0.9
ViT-L FPN	35.3 ± 0.7	57.3 ± 0.6	29.7 ± 0.6	50.1 ± 0.2	31.1 ± 0.8	52.3 ± 0.9	31.2 ± 0.4	52.2 ± 0.5

Table 5. Zero-shot instance detection results for different query levels for FPN models from Sec. 5.2 trained and evaluated on PACO-LVIS.

Model	$L1_{obj}$	$L1_{part}$	L1
MDETR R101	4.1 ± 0.6	5.3 ± 0.6	4.9 ± 0.3
R101 FPN (Ours)	20.3 ± 0.9	24.4 ± 1.0	23.1 ± 0.7
Detic Swin-B	5.2 ± 0.7	6.2 ± 0.3	5.9 ± 0.2
ViT-B FPN (Ours)	22.6 ± 0.8	28.9 ± 0.6	26.8 ± 0.2

Table 6. Zero-shot instance detection performance of open-vocabulary detectors on PACO-LVIS. This is a difficult task for existing methods. We compare AR@1 on a subset of queries that are the closest to the detection task: L1 queries additionally split into subsets with only object ($L1_{obj}$) and only part ($L1_{part}$) attributes.

5.3. Zero-shot instance detection

We generate benchmark numbers for this task by directly leveraging the models trained in Sec. 5.2. For a given query, we use the scores corresponding to the object, part, object attributes, and part attributes mentioned in the query to rank object bounding boxes returned by the different joint models. We use a simple scoring function that combines these different scores using geometric mean to get one final score for each box (explained in the appendix). The results for FPN models trained and evaluated on PACO-LVIS are shown in Tab. 5 (see appendix for cascade model results). We notice an interesting trend. For all models, $L1 > L3 > L2$. This is due to the trade-off between two opposing factors: (a) more complex queries provide more information about the object instance, making L3 task easier than L2, but (b) complex queries also cause errors from multiple attribute predictions to be compounded making L1 better than L3. We include ablation studies in appendix measuring importance of different object and part attributes.

Comparison with open vocabulary detectors

To get a sense of the gap between open vocabulary detectors and our task-specific models, we evaluate the publicly available models from Detic [55] and MDETR [22] without further fine-tuning on PACO-LVIS and report results in Tab. 6 (details in the appendix). In theory, such models can handle arbitrary natural language queries describing object instances. We show results only for L1 queries and two additional subsets: L1 queries with only object attributes ($L1_{obj}$) and only part attributes ($L1_{part}$). We observe limited performance for the evaluated models. This is not surprising and can be attributed to the following factors. Even in the open vocabulary setting, Detic was trained specif-

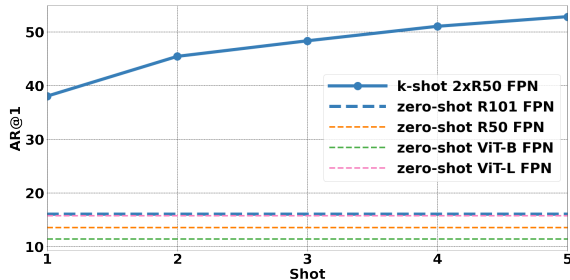


Figure 3. Comparing performance of few-shot model with our zero-shot models on PACO-EGO4D instance detection task. Even at 1-shot we observe a huge gap compared to all zero-shot models.

ically for nouns with little support for attributes. While MDETR was trained for referring expression tasks with attributes, its ability to handle negative images is limited. This highlights the opportunity for future research in open world detectors to handle more descriptive object queries besides category labels.

Comparison with few-shot models on PACO-EGO4D

PACO-EGO4D has multiple frames corresponding to the same object instance. Hence, it can serve as a useful dataset for few-shot instance detection as well. Few-shot instance detection is the task where an algorithm is given as input k positive frames with bounding boxes for an object instance and is expected to retrieve another bounding box of the same instance from an unseen set of images. This is similar to our zero-shot task, but the model receives sample object boxes instead of a part/attribute query. We compute and compare zero-shot and few-shot numbers on a subset of 1992 queries in PACO-EGO4D that have 6 or more boxes for the object instance corresponding to the query. We benchmark a naive 2-stage model: a pre-trained R50 FPN detector followed by ROI-pooling features from a pre-trained R50 FPN backbone for nearest neighbor ranking (explained in appendix). We evaluate this model for k ranging from 1-5 and compare it to our zero-shot instance detection models trained on the joint PACO dataset in Fig. 3. We notice a 20+ point gap even between our best zero-shot model (R101 FPN) and one-shot model ($k = 1$). As k increases, the gap widens even further. This shows scope for future improvements to zero-shot object instance detection.

6. Conclusion

We introduced PACO, a dataset designed to enable research towards joint detection of objects, parts and attributes of common objects. It provides part masks and attributes for 75 common object categories spanning both image and video datasets. We introduce three benchmark tasks which showcase unique challenges in the dataset. Unlike object detection, these tasks require algorithms to cope better with smaller masks belonging to parts and have features that are not invariant to instance-level attributes. For all tasks, we provide results from extensions of existing detection models to help calibrate future research on the dataset.

References

- [1] Zhaowei Cai and Nuno Vasconcelos. Cascade r-cnn: Delving into high quality object detection. In *Proceedings of the IEEE conference on computer vision and pattern recognition*, pages 6154–6162, 2018. [7](#)
- [2] Mathilde Caron, Hugo Touvron, Ishan Misra, Hervé Jégou, Julien Mairal, Piotr Bojanowski, and Armand Joulin. Emerging properties in self-supervised vision transformers. In *Proceedings of the International Conference on Computer Vision (ICCV)*, 2021. [13](#)
- [3] Xianjie Chen, Roozbeh Mottaghi, Xiaobai Liu, Sanja Fidler, Raquel Urtasun, and Alan Yuille. Detect what you can: Detecting and representing objects using holistic models and body parts. In *Proceedings of the IEEE conference on computer vision and pattern recognition*, pages 1971–1978, 2014. [1](#), [2](#)
- [4] Zhenfang Chen, Peng Wang, Lin Ma, Kwan-Yee K. Wong, and Qi Wu. Cops-ref: A new dataset and task on compositional referring expression comprehension. In *Proceedings of the IEEE/CVF Conference on Computer Vision and Pattern Recognition (CVPR)*, June 2020. [1](#), [3](#), [6](#)
- [5] Jia Deng, Wei Dong, Richard Socher, Li-Jia Li, Kai Li, and Li Fei-Fei. Imagenet: A large-scale hierarchical image database. In *2009 IEEE conference on computer vision and pattern recognition*, pages 248–255. Ieee, 2009. [2](#)
- [6] Jiankang Deng, Jia Guo, Niannan Xue, and Stefanos Zafeiriou. Arcface: Additive angular margin loss for deep face recognition. In *Proceedings of the IEEE/CVF conference on computer vision and pattern recognition*, pages 4690–4699, 2019. [18](#)
- [7] Li Deng. The mnist database of handwritten digit images for machine learning research [best of the web]. *IEEE signal processing magazine*, 29(6):141–142, 2012. [2](#)
- [8] N. Dinesh Reddy, Minh Vo, and Srinivasa G. Narasimhan. Carfusion: Combining point tracking and part detection for dynamic 3d reconstruction of vehicles. In *The IEEE Conference on Computer Vision and Pattern Recognition (CVPR)*, June 2018. [2](#)
- [9] M. Everingham, S. M. A. Eslami, L. Van Gool, C. K. I. Williams, J. Winn, and A. Zisserman. The pascal visual object classes challenge: A retrospective. *International Journal of Computer Vision*, 111(1):98–136, Jan. 2015. [2](#)
- [10] Chengjian Feng, Yujie Zhong, Zequn Jie, Xiangxiang Chu, Haibing Ren, Xiaolin Wei, Weidi Xie, and Lin Ma. Prompt-det: Expand your detector vocabulary with uncurated images. *arXiv preprint arXiv:2203.16513*, 2022. [1](#)
- [11] Golnaz Ghiasi, Yin Cui, Aravind Srinivas, Rui Qian, Tsung-Yi Lin, Ekin D Cubuk, Quoc V Le, and Barret Zoph. Simple copy-paste is a strong data augmentation method for instance segmentation. In *Proceedings of the IEEE/CVF Conference on Computer Vision and Pattern Recognition*, pages 2918–2928, 2021. [7](#)
- [12] Ke Gong, Xiaodan Liang, Dongyu Zhang, Xiaohui Shen, and Liang Lin. Look into person: Self-supervised structure-sensitive learning and a new benchmark for human parsing. In *Proceedings of the IEEE conference on computer vision and pattern recognition*, pages 932–940, 2017. [2](#)
- [13] Kristen Grauman, Andrew Westbury, Eugene Byrne, Zachary Chavis, Antonino Furnari, Rohit Girdhar, Jackson Hamburger, Hao Jiang, Miao Liu, Xingyu Liu, et al. Ego4d: Around the world in 3,000 hours of egocentric video. In *Proceedings of the IEEE/CVF Conference on Computer Vision and Pattern Recognition*, pages 18995–19012, 2022. [2](#), [3](#)
- [14] Sheng Guo, Weilin Huang, Xiao Zhang, Prasanna Srikhanta, Yin Cui, Yuan Li, Hartwig Adam, Matthew R Scott, and Serge Belongie. The imaterialist fashion attribute dataset. In *Proceedings of the IEEE/CVF International Conference on Computer Vision Workshops*, pages 0–0, 2019. [2](#)
- [15] Agrim Gupta, Piotr Dollar, and Ross Girshick. LVIS: A dataset for large vocabulary instance segmentation. In *Proceedings of the IEEE Conference on Computer Vision and Pattern Recognition*, 2019. [2](#), [3](#), [5](#), [6](#), [15](#)
- [16] Akshita Gupta, Sanath Narayan, KJ Joseph, Salman Khan, Fahad Shahbaz Khan, and Mubarak Shah. Ow-detr: Open-world detection transformer. In *Proceedings of the IEEE/CVF Conference on Computer Vision and Pattern Recognition*, pages 9235–9244, 2022. [1](#)
- [17] Ju He, Shuo Yang, Shaokang Yang, Adam Kortylewski, Xiaoding Yuan, Jie-Neng Chen, Shuai Liu, Cheng Yang, and Alan Yuille. Partimagenet: A large, high-quality dataset of parts. *arXiv preprint arXiv:2112.00933*, 2021. [1](#), [2](#)
- [18] Kaiming He, Georgia Gkioxari, Piotr Dollár, and Ross Girshick. Mask r-cnn. In *Proceedings of the IEEE international conference on computer vision*, pages 2961–2969, 2017. [2](#), [18](#)
- [19] Drew A Hudson and Christopher D Manning. Gqa: A new dataset for real-world visual reasoning and compositional question answering. In *Proceedings of the IEEE/CVF conference on computer vision and pattern recognition*, pages 6700–6709, 2019. [1](#), [3](#)
- [20] Menglin Jia, Mengyun Shi, Mikhail Sirotenko, Yin Cui, Claire Cardie, Bharath Hariharan, Hartwig Adam, and Serge Belongie. Fashionpedia: Ontology, segmentation, and an attribute localization dataset. In *European conference on computer vision*, pages 316–332. Springer, 2020. [1](#), [2](#), [3](#)
- [21] Licheng Jiao, Ruohan Zhang, Fang Liu, Shuyuan Yang, Biao Hou, Lingling Li, and Xu Tang. New generation deep learning for video object detection: A survey. *IEEE Transactions on Neural Networks and Learning Systems*, 2021. [2](#)

- [22] Aishwarya Kamath, Mannat Singh, Yann LeCun, Gabriel Synnaeve, Ishan Misra, and Nicolas Carion. Mdetmodulated detection for end-to-end multi-modal understanding. In *Proceedings of the IEEE/CVF International Conference on Computer Vision*, pages 1780–1790, 2021. 1, 8, 17
- [23] Sahar Kazemzadeh, Vicente Ordonez, Mark Matten, and Tamara Berg. Referitgame: Referring to objects in photographs of natural scenes. In *Proceedings of the 2014 conference on empirical methods in natural language processing (EMNLP)*, pages 787–798, 2014. 1, 3, 6
- [24] Ronak Kosti, Jose M Alvarez, Adria Recasens, and Agata Lapedriza. Emotion recognition in context. In *Proceedings of the IEEE conference on computer vision and pattern recognition*, pages 1667–1675, 2017. 2
- [25] Ranjay Krishna, Yuke Zhu, Oliver Groth, Justin Johnson, Kenji Hata, Joshua Kravitz, Stephanie Chen, Yannis Kalantidis, Li-Jia Li, David A Shamma, et al. Visual genome: Connecting language and vision using crowdsourced dense image annotations. *International journal of computer vision*, 123(1):32–73, 2017. 1
- [26] Alina Kuznetsova, Hassan Rom, Neil Alldrin, Jasper Uijlings, Ivan Krasin, Jordi Pont-Tuset, Shahab Kamali, Stefan Popov, Matteo Mallocci, Alexander Kolesnikov, et al. The open images dataset v4. *International Journal of Computer Vision*, 128(7):1956–1981, 2020. 2
- [27] Dangwei Li, Zhang Zhang, Xiaotang Chen, Haibin Ling, and Kaiqi Huang. A richly annotated dataset for pedestrian attribute recognition. *arXiv preprint arXiv:1603.07054*, 2016. 1
- [28] Jianshu Li, Jian Zhao, Yunchao Wei, Congyan Lang, Yidong Li, Terence Sim, Shuicheng Yan, and Jiashi Feng. Multiple-human parsing in the wild. *arXiv preprint arXiv:1705.07206*, 2017. 2
- [29] Yining Li, Chen Huang, Chen Change Loy, and Xiaoou Tang. Human attribute recognition by deep hierarchical contexts. In *European conference on computer vision*, pages 684–700. Springer, 2016. 2
- [30] Yanghao Li, Hanzi Mao, Ross B. Girshick, and Kaiming He. Exploring plain vision transformer backbones for object detection. *ArXiv*, abs/2203.16527, 2022. 2, 7, 14
- [31] Tsung-Yi Lin, Piotr Dollár, Ross Girshick, Kaiming He, Bharath Hariharan, and Serge Belongie. Feature pyramid networks for object detection. In *Proceedings of the IEEE conference on computer vision and pattern recognition*, pages 2117–2125, 2017. 7, 19
- [32] Tsung-Yi Lin, Michael Maire, Serge Belongie, James Hays, Pietro Perona, Deva Ramanan, Piotr Dollár, and C Lawrence Zitnick. Microsoft coco: Common objects in context. In *European conference on computer vision*, pages 740–755. Springer, 2014. 2
- [33] Ziwei Liu, Ping Luo, Shi Qiu, Xiaogang Wang, and Xiaoou Tang. Deepfashion: Powering robust clothes recognition and retrieval with rich annotations. In *Proceedings of the IEEE conference on computer vision and pattern recognition*, pages 1096–1104, 2016. 2
- [34] Junhua Mao, Jonathan Huang, Alexander Toshev, Oana Camburu, Alan L Yuille, and Kevin Murphy. Generation and comprehension of unambiguous object descriptions. In *Proceedings of the IEEE conference on computer vision and pattern recognition*, pages 11–20, 2016. 1, 3, 6
- [35] Panagiotis Meletis, Xiaoxiao Wen, Chenyang Lu, Daan de Geus, and Gijs Dubbelman. Cityscapes-panoptic-parts and pascal-panoptic-parts datasets for scene understanding. *arXiv preprint arXiv:2004.07944*, 2020. 2
- [36] Genevieve Patterson and James Hays. Coco attributes: Attributes for people, animals, and objects. *European Conference on Computer Vision*, 2016. 2
- [37] Khoi Pham, Kushal Kafle, Zhe Lin, Zhihong Ding, Scott Cohen, Quan Tran, and Abhinav Shrivastava. Learning to predict visual attributes in the wild. In *Proceedings of the IEEE/CVF Conference on Computer Vision and Pattern Recognition*, pages 13018–13028, 2021. 1, 3
- [38] Shaoqing Ren, Kaiming He, Ross Girshick, and Jian Sun. Faster r-cnn: Towards real-time object detection with region proposal networks. *Advances in neural information processing systems*, 28, 2015. 19
- [39] Bernardino Romera-Paredes and Philip Torr. An embarrassingly simple approach to zero-shot learning. In *International conference on machine learning*, pages 2152–2161. PMLR, 2015. 3
- [40] Shuai Shao, Zeming Li, Tianyuan Zhang, Chao Peng, Gang Yu, Xiangyu Zhang, Jing Li, and Jian Sun. Objects365: A large-scale, high-quality dataset for object detection. In *Proceedings of the IEEE/CVF international conference on computer vision*, pages 8430–8439, 2019. 2
- [41] Amanpreet Singh, Ronghang Hu, Vedanuj Goswami, Guillaume Couairon, Wojciech Galuba, Marcus Rohrbach, and Douwe Kiela. Flava: A foundational language and vision alignment model. In *Proceedings of the IEEE/CVF Conference on Computer Vision and Pattern Recognition*, pages 15638–15650, 2022. 7
- [42] Amanpreet Singh, Guan Pang, Mandy Toh, Jing Huang, Wojciech Galuba, and Tal Hassner. Textocr: Towards large-scale end-to-end reasoning for arbitrary-shaped scene text. In *Proceedings of the IEEE/CVF conference on computer vision and pattern recognition*, pages 8802–8812, 2021. 2
- [43] Xibin Song, Peng Wang, Dingfu Zhou, Rui Zhu, Chenye Guan, Yuchao Dai, Hao Su, Hongdong Li, and Ruigang Yang. Apollocar3d: A large 3d car instance understanding benchmark for autonomous driving. In *Proceedings of the IEEE/CVF Conference on Computer Vision and Pattern Recognition*, pages 5452–5462, 2019. 2
- [44] Andreas Veit, Tomas Matera, Lukas Neumann, Jiri Matas, and Serge Belongie. Coco-text: Dataset and benchmark for text detection and recognition in natural images. *arXiv preprint arXiv:1601.07140*, 2016. 2, 4, 5, 6, 7
- [45] Catherine Wah, Steve Branson, Peter Welinder, Pietro Perona, and Serge Belongie. The caltech-ucsd birds-200-2011 dataset. 2011. 1, 2
- [46] Chenyun Wu, Zhe Lin, Scott Cohen, Trung Bui, and Subhransu Maji. Phrasecut: Language-based image segmentation in the wild. In *Proceedings of the IEEE/CVF Conference on Computer Vision and Pattern Recognition*, pages 10216–10225, 2020. 3

- [47] Yuxin Wu, Alexander Kirillov, Francisco Massa, Wan-Yen Lo, and Ross Girshick. Detectron2. <https://github.com/facebookresearch/detectron2>, 2019. 19
- [48] Yongqin Xian, Bernt Schiele, and Zeynep Akata. Zero-shot learning-the good, the bad and the ugly. In *Proceedings of the IEEE conference on computer vision and pattern recognition*, pages 4582–4591, 2017. 3
- [49] Ke Yan, Youbao Tang, Yifan Peng, Veit Sandfort, Mohammadhadi Bagheri, Zhiyong Lu, and Ronald M Summers. Mulan: multitask universal lesion analysis network for joint lesion detection, tagging, and segmentation. In *International Conference on Medical Image Computing and Computer-Assisted Intervention*, pages 194–202. Springer, 2019. 2
- [50] Lu Yang, Qing Song, Zhihui Wang, and Ming Jiang. Parsing r-cnn for instance-level human analysis. In *Proceedings of the IEEE/CVF Conference on Computer Vision and Pattern Recognition*, pages 364–373, 2019. 2
- [51] Shuai Zheng, Fan Yang, M Hadi Kiapour, and Robinson Piramuthu. Modanet: A large-scale street fashion dataset with polygon annotations. In *Proceedings of the 26th ACM international conference on Multimedia*, pages 1670–1678, 2018. 1, 2
- [52] Bolei Zhou, Agata Lapedriza, Aditya Khosla, Aude Oliva, and Antonio Torralba. Places: A 10 million image database for scene recognition. *IEEE transactions on pattern analysis and machine intelligence*, 40(6):1452–1464, 2017. 2
- [53] Bolei Zhou, Hang Zhao, Xavier Puig, Sanja Fidler, Adela Barriuso, and Antonio Torralba. Scene parsing through ade20k dataset. In *Proceedings of the IEEE conference on computer vision and pattern recognition*, pages 633–641, 2017. 2
- [54] Bolei Zhou, Hang Zhao, Xavier Puig, Tete Xiao, Sanja Fidler, Adela Barriuso, and Antonio Torralba. Semantic understanding of scenes through the ade20k dataset. *International Journal of Computer Vision*, 127(3):302–321, 2019. 1, 2
- [55] Xingyi Zhou, Rohit Girdhar, Armand Joulin, Phillip Krähenbühl, and Ishan Misra. Detecting twenty-thousand classes using image-level supervision. *arXiv preprint arXiv:2201.02605*, 2022. 1, 8, 17
- [56] Xizhou Zhu, Weijie Su, Lewei Lu, Bin Li, Xiaogang Wang, and Jifeng Dai. Deformable detr: Deformable transformers for end-to-end object detection. *arXiv preprint arXiv:2010.04159*, 2020. 7

Appendix

A. Dataset construction

A.1. Parts vocabulary selection

We show sample images obtained by querying the web for “parts of an object category” for different object categories in Fig. 4. We see that the images provide a good vocabulary of parts for each of the objects. Alongside, they also provide clear pointers to the regions of the object the parts correspond to. We use these as reference images for annotators wherever such well defined part images are available from the web. Additionally, we also manually define

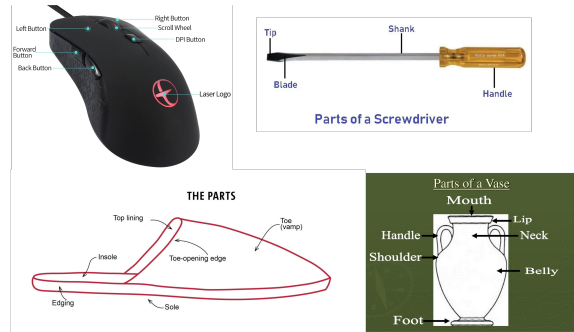


Figure 4. Sample web images used to mine part vocabulary. top-left: “Parts of a computer mouse”, top-right: “Parts of a screw-driver”, bottom-left: “Parts of a slipper” and bottom-right: “Parts of a vase”.

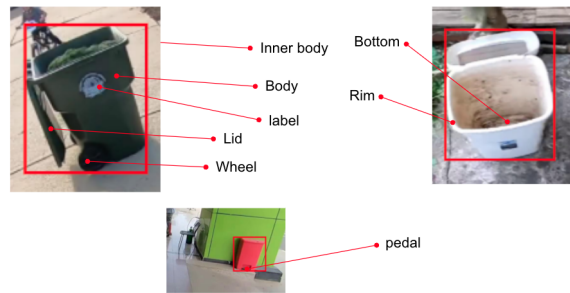


Figure 5. Example object category with manually defined parts. For the object “trash can”, we manually defined all the parts with illustrative reference for the annotators as shown.

parts for few objects when the web images aren’t illustrative enough. In such cases, we came up with reasonable names for different regions of an object along with reference images to guide the annotators. Such manually defined parts with sample reference images are shown in Fig. 5 as well. Tab. 7 contains the final taxonomy of parts for the 75 object classes.

A.2. Attribute vocabulary selection

For zero-shot instance recognition tasks, both object and part level attributes are important. In order to identify the set of attributes that we should annotate that are sufficient for the tasks, we conducted an in-depth user study.

We consider the following 5 attributes types: color, shape, reflectance, materials and patterns & marking with the aim of finding a small subset that is sufficient to discriminate between the instances. We show each user two different instances A and B of the same object (green mug and red mug for example), segmentation mask of common object parts between this pair. We use PACO-Ego4D data for this purpose. For object level attributes, we ask annotators to provide at most one difference (if any) for each attribute type. For part level attributes, annotators are asked

Objects	Parts Taxonomy
basket	bottom, handle, inner_side, cover, side, rim, base
belt	buckle, end_tip, strap, frame, bar, prong, loop, hole
bench	stretcher, seat, back, table_top, leg, arm
bicycle	stem, fork, top_tube, wheel, basket, seat_stay, saddle, handlebar, pedal, gear, head_tube, down_tube, seat_tube
blender	cable, handle, cover, spout, vapour_cover, base, inner_body, seal_ring, cup, switch, food_cup
book	page, cover
bottle	neck, label, shoulder, body, cap, bottom, inner_body, closure, heel, top, handle, ring, sipper, capsule, spout, base, punt
bowl	inner_body, bottom, body, rim, base
box	bottom, lid, inner_side, side
broom	lower_bristles, handle, brush_cap, ring, shaft, brush
bucket	handle, cover, body, base, inner_body, bottom, loop, rim
calculator	key, body
can	pull_tab, body, base, inner_body, bottom, lid, text, rim
car_(automobile)	headlight, turnsignal, tank, windshield, mirror, sign, wiper, fender, trunk, windowpane, seat, logo, grille, antenna, hood, splashboard, bumper, rim, handle, runningboard, window, roof, wheel, taillight, steeringwheel
carton	inner_side, tapering_top, cap, bottom, lid, text, side, top
cellular_telephone	button, screen, bezel, back_cover
chair	stretcher, swivel, apron, wheel, leg, base, spindle, seat, back, rail, stile, skirt, arm
clock	cable, decoration, hand, pediment, finial, case, base
crate	bottom, handle, inner_side, lid, side
cup	inner_body, handle, rim, base
dog	teeth, neck, foot, head, body, nose, leg, tail, ear, eye
drill	handle, body
drum_(musical_instrument)	head, rim, cover, body, loop, lug, base
earphone	headband, cable, ear_pads, housing, slider
fan	rod, canopy, motor, blade, base, string, light, bracket, fan_box, pedestal_column
glass_(drink_container)	inner_body, bottom, body, rim, base
guitar	key, headstock, bridge, body, fingerboard, back, string, side, pickguard, hole
hammer	handle, face, head, grip
handbag	zip, inner_body, handle, bottom, body, rim, base
hat	logo, pom_pom, inner_side, strap, visor, rim
helmet	face_shield, logo, inner_side, strap, visor, rim
jar	handle, body, base, inner_body, bottom, lid, sticker, text, rim
kettle	cable, handle, lid, body, spout, base
knife	handle, blade
ladder	rail, step, top_cap, foot
lamp	shade_inner_side, cable, pipe, shade, bulb, shade_cap, base, switch, finial
laptop_computer	cable, camera, base_panel, keyboard, logo, back, screen, touchpad
microwave_oven	inner_side, door_handle, time_display, control_panel, turntable, dial, side, top
mirror	frame
mouse_(computer_equipment)	logo, scroll_wheel, body, right_button, wire, side_button, left_button
mug	handle, body, base, inner_body, bottom, text, drawing, rim
newspaper	text
pan_(for_cooking)	bottom, handle, inner_side, lid, side, rim, base
pen	cap, grip, barrel, clip, tip
pencil	body, lead, eraser, ferrule
pillow	embroidery
pipe	nozzle, colied_tube, nozzle_stem
plastic_bag	inner_body, handle, text, hem, body
plate	top, bottom, inner_wall, body, rim, base
pliers	jaw, handle, joint, blade
remote_control	logo, back, button
scarf	fringes, body
scissors	handle, screw, finger_hole, blade
screwdriver	blade, handle, tip, shank
shoe	toe_box, tongue, vamp, outsole, insole, backstay, lining, quarter, heel, throat, eyelet, lace, welt
slipper_(footwear)	toe_box, vamp, outsole, strap, insole, lining
soap	neck, label, shoulder, body, sipper, capsule, spout, push_pull_cap, cap, base, bottom, closure, punt, top
sponge	rough_surface
spoon	neck, handle, bowl, tip
stool	seat, leg, step, footrest
sweater	shoulder, sleeve, neckband, hem, body, yoke, cuff
table	stretcher, drawer, inner_wall, shelf, apron, wheel, leg, top, rim
tape_(sticky_cloth_or_paper)	roll
telephone	button, screen, bezel, back_cover
television_set	bottom, button, side, top, base
tissue_paper	roll
towel	body, terry_bar, hem, border
trash_can	label, body, wheel, inner_body, bottom, lid, pedal, rim, hole
tray	bottom, inner_side, outer_side, rim, base
vase	neck, handle, foot, body, mouth
wallet	inner_body, flap
watch	buckle, case, dial, hand, strap, window, lug
wrench	handle, head

Table 7. Parts taxonomy

to compare only between the common parts of the instance pair and they are allowed to annotate up to 3 part level at-

Attribute Type	Attribute Classes
Color	black, light_blue, blue, dark_blue, light_brown, brown, dark_brown, light_green, green, dark_green, light_grey, grey, dark_grey, light_orange, orange, dark_orange, light_pink, pink, dark_pink, light_purple, purple, dark_purple, light_red, red, dark_red, white, light_yellow, yellow, dark_yellow
Pattern-Markings	plain, striped, dotted, checkered, woven, studded, perforated, floral, logo, text
Material	stone, wood, rattan, fabric, crochet, wool, leather, velvet, metal, paper, plastic, glass, ceramic
Reflectance	opaque, translucent, transparent

Table 8. Attributes taxonomy

tribute differences for one pair. For an attribute difference, if the discriminative attributes for A and B is nameable (e.g. A is red and B is blue), annotators will need to write down the attribute names. Otherwise, a freeform explanation is required to articulate this difference, particularly for unnameable attributes (e.g. a unique pattern, an irregular shape, etc.); For each object category we sampled 106 pairs each which are annotated by 3 annotators.

Un-nameable shape attributes. Annotators noted that $> 50\%$ shape differences contain unnameable attributes. Annotators reported these differences as very difficult to describe with words. Hence, we removed “shape” from the final list of attribute. Nevertheless, even in the absence of shape we note that the combination of the remaining attributes are seen to be sufficiently discriminative to differentiate the object instances.

Attributes Coverage. We try to identify the discriminative power of different subsets of attributes and identify the best subset to construct our attributes taxonomy. We adopted a greedy algorithm to study attribute sets. We start with one attribute and gradually add one best attribute at a time to incrementally construct an attribute set at each step. More specifically at a give step, for each attribute, we check how many new pairs can be distinguished if we introduce that attribute to the existing set of attributes. The attribute that distinguishes highest number of pairs is selected first, followed by the next best attribute in a greedy fashion. We define coverage of a set of attributes as the total number of object pairs that can be distinguished by the attributes (both with object-level attributes and/or part-level attributes).

We observed that coverage plateaus at 40 attributes. 98% of object instance pairs could be distinguished only using the 55 attributes included in our final version of PACO. Both object and part attributes were marked as important for differentiating instance pairs. 18% instance pairs could only be distinguished by object level attributes, while 10% could only be distinguished by part level attributes. Color is the biggest discriminative attribute type for instance recognition, differentiating at least 75% instance pairs with both object and part level color differences.

The final taxonomy of attributes is shown in Tab. 8.

A.3. Annotation pipeline

A.3.1 Instance annotation

To enable appearance based k-shot instance detection experiments we have annotated instances with unique instance IDs. For LVIS (image) dataset, we assume image of each object to be a separate instance. We inspected several images manually and found this assumption to be true. In Ego4D videos from which we sourced the frames, however, the same instance can occur multiple times at different timestamps and we had to set up an annotation task to properly group occurrences (frames) into instances. There are two challenges that we faced: (a) the same video can contain different instances of the same object class and those have to be split into separate instance IDs, and (b) Ego4D videos are fragmented and multiple videos can contain the same instances so occurrences from different videos had to be merged. To this end we performed a three-step splitting/merging annotation pipeline as follows.

Split: Using (video, category) pair as a good first guess for instance ID, we crop all the bounding boxes (occurrences) of an object category from frames that belong to the same video and show them to annotators. We then ask the annotators to split those crops into subgroups that belong to the same real instance. In case number of boxes is more than 16, we split them in to groups of at most 16 and then send them for annotation. This is then repeated for all object categories and all videos. All annotation jobs are reviewed by 3 annotators and a subset majority voting is performed to aggregate annotations. The majority voting is done by finding the maximum overlap between subgroups for each pair of annotators using Hungarian algorithm (bipartite matching).

Merge: After the splitting phase the annotated groups are very coherent, i.e., the majority of occurrences in the same group belong to the same instance. However due to video fragmentation and additional limitation on the number of boxes that can be shown to annotators (16) many occurrence groups belong to the same instance and need to be merged. To address this we use similarity in DINO model [2] embedding space. Each group from the splitting phase is represented by a bounding box crop with embedding closest to the group median. For each group

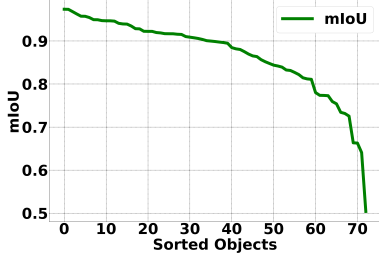


Figure 6. Distribution of mIoU with gold-standard part masks for different object classes. 90% of the object classes have mIoU \geq 0.75 with the gold-standard masks.

representative g_i we find 16 nearest neighbors and ask annotators to validate which of the neighbors belong to the same instance as g_i . Similar to the splitting phase, responses from 3 annotators are aggregated by finding the maximum overlap between any two annotators. We repeat this for every group. We then build a graph by considering each group as a node with an edge between two nodes if they belong to the same instance. Nodes i and j are connected if g_j was marked as belonging to the same instance as g_i **and** g_i was marked as belonging to the same instance as g_j . Finally, we find connected components and assign a unique instance ID to each component.

Final split: We noticed some over-merging of instances, especially for instances with large number of occurrences. We therefore performed a third step where we showed instances with more than 10 occurrences to expert annotators and asked them to split them into subgroups. Each subgroup at the output of this step is then marked as a separate instance. There was no limit of 16 occurrences in this step, complete instances were shown in each annotation job.

A.3.2 Managing annotation quality

Fig. 6 shows the mIoU of annotated masks with gold set masks for each object category.

B. Dataset annotation examples

Object, part, and attribute annotations are shown in Figs. 7 and 12. Object and part segmentation masks are used to crop out segments for annotations with a specific attribute and shown in Fig. 7 for a subset of attributes. Fig. 12 shows various examples for PACO annotations. Full images are shown with object annotations (bounding boxes only so attributes are visible) in the left copy of the image and part annotations (segmentation masks) in the right copy of the image. Object and part attribute annotations are listed below each image pair.

Model	mask AP		box AP	
	AP^{obj}	AP^{opart}	AP^{obj}	AP^{opart}
R50 FPN	31.2 ± 0.1	12.1 ± 0.1	34.3 ± 0.2	15.7 ± 0.2
R101 FPN	32.0 ± 0.3	12.5 ± 0.1	35.2 ± 0.3	16.2 ± 0.2
ViT-B FPN	35.5 ± 0.5	14.1 ± 0.3	39.2 ± 0.5	18.1 ± 0.5
ViT-L FPN	44.7 ± 0.4	18.1 ± 0.3	49.6 ± 0.4	22.9 ± 0.4

Table 9. Object and object-part segmentation results for mask-RCNN and ViT-det models trained jointly on PACO-LVIS and PACO-EGO4D and evaluated on PACO-LVIS

Model	mask AP		box AP	
	AP^{obj}	AP^{opart}	AP^{obj}	AP^{opart}
R50 FPN	16.6 ± 0.3	5.6 ± 0.0	18.9 ± 0.3	8.2 ± 0.1
R101 FPN	17.9 ± 0.2	6.0 ± 0.1	20.3 ± 0.2	8.7 ± 0.1
ViT-B FPN	18.6 ± 0.2	7.0 ± 0.2	20.7 ± 0.3	10.1 ± 0.1
ViT-L FPN	27.9 ± 0.3	10.5 ± 0.3	30.6 ± 0.2	14.8 ± 0.4

Table 10. Object and object-part segmentation results for mask-RCNN and ViT-det models trained jointly on PACO-LVIS and PACO-EGO4D and evaluated on PACO-EGO4D

C. Object statistics

Fig. 8 shows the distribution of instances across the 75 object categories in PACO-LVIS and PACO-EGO4D. All 75 object classes in PACO-LVIS and 71 classes in PACO-EGO4D have \geq 10 instances. We observe the usual non-uniformity in the frequency for each category. For object category ‘drill’ with the lowest frequency in PACO-LVIS, we have 23 instances, and for ‘scarf’ with the lowest frequency in PACO-EGO4D data, we have 7 instances.

D. Additional part segmentation and attribute prediction results

In Fig. 9, we show the architecture of the models used to train the joint segmentation and attribute prediction models. For our experiments, we vary the backbones across R-50, R-101 and two ViT-det [30] model backbones.

Examples of predictions from the ViT-L model are shown in Fig. 13.

D.1. Joint training on PACO-LVIS and PACO-EGO4D

In addition to models trained on PACO-LVIS, we also train models for part segmentation and attribute prediction jointly trained on both PACO-LVIS and PACO-EGO4D. We evaluate the jointly trained models on the test splits for both the datasets and present the results for part segmentation in Tab. 9 and Tab. 10. Tab. 11 and Tab. 12 show the results on attribute prediction. We notice that the results on PACO-EGO4D overall are lower compared to those for PACO-LVIS. This is indicative of the challenges in video domain particularly for ego-centric videos. Also, we note that the jointly trained model offers a small improvement compared



Figure 7. Randomly sampled object (top row) and part (bottom row) masks for a subset of attributes (one attribute per column).

Model	AP_{att}^{obj}	AP_{col}^{obj}	AP_{pat}^{obj}	AP_{mat}^{obj}	AP_{ref}^{obj}	AP_{att}^{opart}	AP_{col}^{opart}	AP_{pat}^{opart}	AP_{mat}^{opart}	AP_{ref}^{opart}
R50 FPN	13.8 ± 0.1	10.6 ± 0.4	14.9 ± 0.7	9.7 ± 0.2	19.8 ± 0.9	9.7 ± 0.1	10.3 ± 0.5	10.7 ± 0.5	7.2 ± 0.2	10.7 ± 0.2
R101 FPN	14.0 ± 0.4	11.2 ± 0.3	14.2 ± 0.9	9.8 ± 0.4	20.6 ± 1.6	10.1 ± 0.2	10.8 ± 0.4	11.0 ± 0.3	7.2 ± 0.0	11.3 ± 0.3
ViT-B FPN	16.2 ± 0.6	13.2 ± 0.4	16.7 ± 0.9	13.3 ± 0.3	21.4 ± 1.4	11.5 ± 0.1	12.0 ± 0.1	12.6 ± 0.2	9.4 ± 0.0	11.8 ± 0.4
ViT-L FPN	18.8 ± 0.7	15.6 ± 0.2	19.6 ± 1.1	15.7 ± 0.6	24.5 ± 1.2	14.1 ± 0.1	15.0 ± 0.3	15.2 ± 0.7	11.6 ± 0.1	14.3 ± 0.2

Table 11. Attribute prediction results for a mask R-CNN and ViT-det model trained jointly on PACO-LVIS and PACO-EGO4D and evaluated on PACO-LVIS. The results are shown for box AP for both object attributes and object-part attributes prediction.

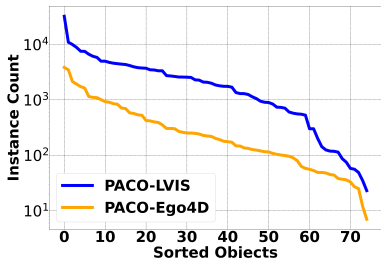


Figure 8. Distribution of instances across the 75 object categories.

to model trained only on PACO-LVIS, when evaluate on PACO-LVIS in Tab. 11. We observed 0.2% gain for R50-FPN and R101-FPN and 0.8% improvement for ViT-B FPN, compared to model trained only with PACO-LVIS.

D.2. val to test results transfer

Here, we wish to study if observations made from the `val` split are similar to the `test` split. This would help us verify if `val` split can be used for model tuning. In Tab. 13 and Tab. 14, we observe that the ranking of results is consistent across `val` and `test`. Across different architectures the trends are similar. This study is similar to what is reported in LVIS [15] for object detection.

D.3. Object segmentation only models

In this section, we explore the effect of joint training on multiple tasks (segmentation and attribute prediction) together on object segmentation results. As an ablation, we train models on only the task of object segmentation for

two backbones: R-50 and ViT-L. We report our observations in Tab. 15. For the smaller R-50 backbone, the object segmentation performance deteriorates slightly when joint training with multiple tasks. However, surprisingly for the higher capacity ViT-L backbone, object segmentation improves considerably when training on the joint task.

D.4. Attribute prediction bounds

In the main paper, we report the bounds on AP_{att}^{obj} . The lower bound is calculated by assuming that the score for the object-attribute prediction is the same as the score for the object prediction, i.e., the lower bound performance is the same as if only the detector was used for attribute prediction. The upper bound performance assumes perfect attribute prediction by setting the score for gt attribute to 1.0 and any false positive attribute predictions to 0.0 for a given object prediction. Here, object refers to both object and object-parts.

E. Additional zero-shot instance detection results

We show results for FPN and cascade models trained and evaluated on PACO-LVIS in Tab. 16. Cascade models improve the performance for all but the largest model. In Tab. 17 we also show the results from models trained on the joint PACO dataset and evaluated on PACO-LVIS and PACO-EGO4D test sets. PACO-EGO4D is a more challenging dataset, zero-shot results are in line with attributes prediction results shown in Tab. 12.

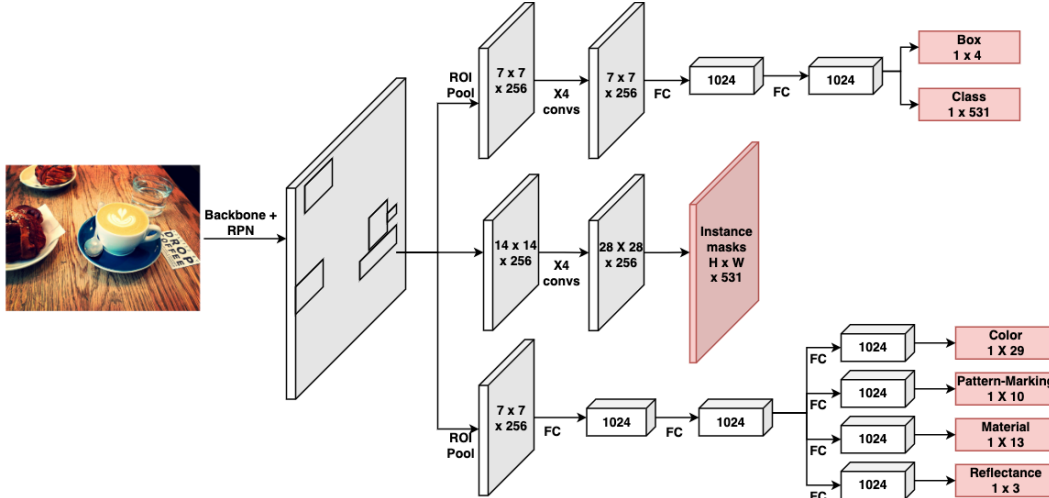


Figure 9. Our model adds an attribute prediction head to Mask R-CNN for joint instance segmentation with attribute prediction

Model	AP_{att}^{obj}	AP_{col}^{obj}	AP_{pat}^{obj}	AP_{mat}^{obj}	AP_{ref}^{obj}	AP_{att}^{part}	AP_{col}^{part}	AP_{pat}^{part}	AP_{mat}^{part}	AP_{ref}^{part}
R50 FPN	6.6 ± 0.4	5.2 ± 0.2	7.0 ± 0.3	6.6 ± 0.8	7.7 ± 0.4	5.6 ± 0.1	5.6 ± 0.5	6.6 ± 0.6	5.7 ± 0.3	4.5 ± 0.3
R101 FPN	7.3 ± 0.2	5.4 ± 0.2	7.6 ± 0.3	8.1 ± 0.5	8.2 ± 0.4	5.9 ± 0.1	5.7 ± 0.6	7.0 ± 1.1	6.1 ± 0.3	4.6 ± 0.3
ViT-B FPN	8.6 ± 0.1	6.6 ± 0.5	10.8 ± 0.7	8.7 ± 0.3	8.2 ± 0.7	7.3 ± 0.1	6.2 ± 0.8	10.7 ± 0.4	6.8 ± 0.6	5.7 ± 0.0
ViT-L FPN	11.7 ± 0.3	9.0 ± 0.1	13.1 ± 1.5	12.4 ± 0.2	12.4 ± 0.4	10.0 ± 0.5	7.8 ± 0.6	12.6 ± 2.0	9.9 ± 0.2	9.7 ± 0.3

Table 12. Attribute prediction results for a mask R-CNN and ViT-det model trained jointly on PACO-LVIS and PACO-EGO4D and evaluated on PACO-EGO4D. The results are shown for box AP for both object attributes and object-part attributes prediction.

Model	split	AP^{obj}	AP^{part}	AP_{att}^{obj}	AP_{att}^{part}
R50 FPN	val	38.3 ± 0.4	18.4 ± 0.3	20.0 ± 0.5	17.1 ± 0.4
	test	34.3 ± 0.2	15.7 ± 0.2	13.8 ± 0.1	9.7 ± 0.1
R101 FPN	val	39.4 ± 0.2	18.7 ± 0.5	21.0 ± 0.9	17.3 ± 0.4
	test	35.2 ± 0.3	16.2 ± 0.2	14.0 ± 0.4	10.1 ± 0.2
ViT-B FPN	val	42.6 ± 0.7	20.8 ± 0.7	25.2 ± 0.5	21.0 ± 0.3
	test	39.2 ± 0.5	18.1 ± 0.5	16.2 ± 0.6	11.5 ± 0.1
ViT-L FPN	val	52.6 ± 0.5	25.9 ± 0.7	29.2 ± 0.6	25.9 ± 0.1
	test	49.6 ± 0.4	22.9 ± 0.4	18.8 ± 0.7	14.1 ± 0.1

Table 13. We compare how object detection, object-part detection and attribute prediction results transfer from val set to test set. The models are trained jointly on PACO-LVIS and PACO-EGO4D and evaluated on PACO-LVIS. The ranking is consistent across both splits

Model	split	AP^{obj}	AP^{part}	AP_{att}^{obj}	AP_{att}^{part}
R50 FPN	val	37.3 ± 0.7	18.6 ± 0.4	28.8 ± 3.3	21.2 ± 3.7
	test	18.9 ± 0.3	8.2 ± 0.1	6.6 ± 0.4	5.6 ± 0.1
R101 FPN	val	38.9 ± 0.3	19.4 ± 0.2	30.5 ± 3.4	22.7 ± 3.0
	test	20.3 ± 0.2	8.7 ± 0.1	7.3 ± 0.2	5.9 ± 0.1
ViT-B FPN	val	48.1 ± 0.3	24.9 ± 0.1	44.3 ± 2.2	35.5 ± 1.0
	test	20.7 ± 0.3	10.1 ± 0.1	8.6 ± 0.1	7.3 ± 0.1
ViT-L FPN	val	56.1 ± 0.1	30.8 ± 0.1	48.8 ± 3.1	39.8 ± 0.7
	test	30.6 ± 0.2	14.8 ± 0.4	11.7 ± 0.3	10.0 ± 0.5

Table 14. We compare how object detection, object-part detection and attribute prediction results transfer from val set to test set. The models are trained jointly on PACO-LVIS and PACO-EGO4D and evaluated on PACO-EGO4D. The ranking is consistent across both splits

F. Ablation studies for zero-shot instance detection

We also measure the importance of different aspects such as object category, object-part category, object colors, part colors and non-color attributes for this end to end task by incrementally including them over a vanilla detection model in Tab. 18. As expected, the object-only performance is poor and each additional component improves the instance detection performance.

G. From model outputs to query scores

For prediction ranking in the zero-shot instance detection task we need query scores for each detected box. However models trained in Sec. 5.2 produce object, part, and attribute scores instead. In this section we provide details of how these scores are used to obtain query scores for each box.

Let Q be a query for an object o , with object-level attributes A , parts P and part-level attributes $A_p \forall p \in P$. For example, the query “Black dog with white ear and brown foot” corresponds to o (dog), object-level attributes

A ({"black"}), parts P ({"ear", "foot"}), part-level attributes A_p ({"white"} for "ear", {"brown"} for "foot").

Given such a query, we assign a query score to all object boxes in an image. This is a two-step process. In the first step, we associate object-parts detected by our model to the corresponding object boxes in the image. In the second step, we calculate the query score for each object box based on the associated parts.

Part association. Since object-part and object boxes are detected independently by our model, we need to associate part boxes to objects first. For a given object box, consider all part boxes where the part class corresponds to the object class of the object box, e.g., for a "car" object box, we will only consider predictions for "car-wheel" and not "bicycle-wheel". From these, select part boxes where more than 50% of the part mask area is contained within the object mask. Call these part boxes matched parts. The matched parts may contain multiple occurrences of the same object-part class, keep only the one with the highest score. This results in set of matched parts for each object box. For some objects, we may have no matched parts for a specific object-part (eg: we may find no "car-wheel" matched with a "car" box).

Query score. For a given object box b , let the predicted score for the query object category o be given by o_o . Similarly, let the predicted object attribute scores be a_k for $k \in A$. Similarly, the part scores of the matched object-parts are given by p_p for $p \in P$. These are the predicted category scores for the matched part box corresponding to each object-part category mentioned in the query. For an object-part category if no part box is matched to b , this score is set to 0. We also have attribute scores for each matched object-part $a_{p,k}$ for $p \in P, k \in A_p$. These scores are again set to 0 if no part box of the corresponding object-part category is matched with b . For the query Q , the score is then computed as follows:

$$s(Q, b) = \begin{cases} \text{if } |A| > 0 : & \sqrt{o_o \times \sqrt{|A|} \prod_{k \in A} a_k} \\ \text{otherwise :} & o_o \\ \times \begin{cases} \text{if } |P| > 0 : & \frac{\sum_{p \in P} \sqrt{p_p \times \sqrt{|A_p|} \prod_{k \in A_p} a_{p,k}}}{|P|} \\ \text{otherwise :} & 1 \end{cases} \end{cases}$$

This is repeated for all queries and all detected boxes.

The above scoring function combines the scores of the object, object-attribute, parts and part-attributes mentioned in the query. Note that the first part of the scoring function only combines object and object-attribute scores, while the second part combines part and part-attribute scores. While combining part scores we use a combination of arithmetic and geometric means. We found this combination to provide the best results empirically.

Model	mask AP AP^{obj}	box AP AP^{obj}
R50 FPN	31.2 ± 0.1	34.3 ± 0.2
R50 FPN - object only	32.4 ± 0.6	35.5 ± 0.5
ViT-L FPN	44.7 ± 0.4	49.6 ± 0.4
ViT-L FPN - object only	39.8 ± 0.1	43.6 ± 0.1

Table 15. Comparison of model performance on object segmentation when trained only on the task of object segmentation vs joint training on object and part segmentation and attribute prediction.

H. Evaluation of open world detectors on zero-shot instance detection task

In this section we give details on how we evaluated Detic [55] and MDETR [22] on zero-shot instance detection task. For both projects we used code open sourced on GitHub.

Detic supports a custom vocabulary and encodes natural language class descriptions using pre-trained CLIP text encoder. We used all 5k queries as custom vocabulary so that we have prediction scores for all queries for each detected box. Due to large vocabulary we had to increase the number of detections per image. We experimented with this parameter and found that 2,000 boxes gives the best results. We used plain query strings (e.g., "A dog with brown ear and black neck") from PACO dataset as class descriptions along with 3 more prompt variants with prefixes "A photo of", "A close up picture of", and "A close up photo of" in front of the plain query strings. The "close up" variants were an attempt to guide text embeddings closer to a detection setup but we didn't see much improvement in performance. We use Detic_LCOCO121k_CLIP_SwinB_896b32_4x_ft4x_max-size.pth model and report mean and standard deviation $AR@k$ calculated over results from these 4 prompt variants.

MDETR is geared towards referring expressions and phrase grounding and treats each image-text pair independently. We follow inference similar to LVIS evaluation reported in the MDETR paper. Namely, for inference on a given image, we evaluate the model on each of the 5k queries separately, then merge the sets of boxes detected on each of the queries and keep the boxes corresponding to top K query scores. Unlike Detic, predicted boxes are not shared across queries since MDETR predicts bounding boxes independently for each query. As a result, we had to increase the number of detections per image even further to 10,000 to obtain the best results. We also experimented with two MDETR models with R101 backbone⁴, one trained for referring expressions task (ref-cocog_resnet101_checkpoint.pth) and the other for LVIS few-shot task (lvis10_checkpoint.pth) and observed that LVIS few-shot task model performs bet-

⁴A known issue (#86) prevented the use of ENB backbones

Model	L1 queries		L2 queries		L3 queries		all queries	
	AR@1	AR@5	AR@1	AR@5	AR@1	AR@5	AR@1	AR@5
R50 FPN	22.5 ± 0.7	39.2 ± 0.5	20.1 ± 0.4	38.5 ± 0.1	22.3 ± 0.9	44.5 ± 1.1	21.4 ± 0.6	40.9 ± 0.3
+ cascade	23.5 ± 1.4	41.1 ± 2.7	21.4 ± 2.4	40.9 ± 3.2	25.3 ± 2.7	48.1 ± 3.2	23.3 ± 2.3	43.7 ± 3.1
R101 FPN	23.1 ± 0.7	40.5 ± 1.4	20.0 ± 0.6	39.3 ± 1.0	23.1 ± 0.7	45.2 ± 0.6	21.7 ± 0.6	41.8 ± 0.8
+ cascade	26.3 ± 0.4	45.1 ± 0.5	24.0 ± 0.1	43.2 ± 0.1	26.6 ± 1.2	49.5 ± 0.8	25.4 ± 0.5	45.9 ± 0.4
ViT-B FPN	26.8 ± 0.2	45.8 ± 0.2	22.7 ± 0.5	40.0 ± 0.7	24.1 ± 0.5	42.5 ± 1.5	23.9 ± 0.4	42.0 ± 0.9
+ cascade	27.0 ± 0.4	46.1 ± 0.5	23.0 ± 0.9	40.3 ± 0.2	25.5 ± 0.8	43.1 ± 0.5	24.7 ± 0.7	42.4 ± 0.2
ViT-L FPN	35.3 ± 0.7	57.3 ± 0.6	29.7 ± 0.6	50.1 ± 0.2	31.1 ± 0.8	52.3 ± 0.9	31.2 ± 0.4	52.2 ± 0.5
+ cascade	33.8 ± 0.7	57.2 ± 0.2	29.0 ± 0.7	50.2 ± 0.2	30.1 ± 0.7	51.8 ± 1.8	30.2 ± 0.6	52.0 ± 0.6

Table 16. Zero-shot instance detection results for different query levels for FPN and cascade models from Sec. 5.2 trained and evaluated on PACO-LVIS.

Model	Eval set	L1 queries		L2 queries		L3 queries		all queries	
		AR@1	AR@5	AR@1	AR@5	AR@1	AR@5	AR@1	AR@5
R50 FPN	PACO-LVIS	22.0 ± 0.4	39.6 ± 0.6	20.6 ± 0.5	39.0 ± 0.7	24.7 ± 1.0	45.5 ± 1.4	22.4 ± 0.3	41.6 ± 0.7
R101 FPN	PACO-LVIS	23.5 ± 0.5	40.9 ± 0.4	21.2 ± 0.3	40.1 ± 0.7	24.3 ± 1.3	45.2 ± 0.9	22.8 ± 0.5	42.2 ± 0.6
ViT-B FPN	PACO-LVIS	29.5 ± 0.6	49.5 ± 1.1	25.8 ± 1.4	44.9 ± 2.3	26.2 ± 1.2	45.7 ± 2.9	26.6 ± 1.1	46.0 ± 2.2
ViT-L FPN	PACO-LVIS	38.0 ± 0.6	60.8 ± 1.2	33.3 ± 1.7	55.6 ± 1.9	33.1 ± 2.6	59.0 ± 2.8	34.0 ± 1.8	57.8 ± 2.1
R50 FPN	PACO-EGO4D	15.4 ± 0.1	29.1 ± 0.6	13.2 ± 0.2	28.0 ± 0.9	14.4 ± 1.8	29.1 ± 1.3	14.2 ± 0.9	28.7 ± 0.8
R101 FPN	PACO-EGO4D	16.3 ± 0.5	29.8 ± 0.9	15.0 ± 0.6	28.6 ± 0.7	14.2 ± 0.6	28.3 ± 0.9	14.9 ± 0.1	28.6 ± 0.5
ViT-B FPN	PACO-EGO4D	13.5 ± 1.2	24.4 ± 1.3	11.0 ± 0.4	19.5 ± 0.7	9.3 ± 0.5	18.1 ± 0.5	10.6 ± 0.1	19.7 ± 0.4
ViT-L FPN	PACO-EGO4D	20.8 ± 0.2	36.9 ± 0.7	19.8 ± 1.3	33.3 ± 1.3	21.4 ± 1.2	34.9 ± 0.7	20.7 ± 1.0	34.7 ± 0.9

Table 17. Zero-shot instance detection results for different query levels for FPN models from Sec. 5.2 trained on joint PACO dataset and evaluated on PACO-LVIS and PACO-EGO4D.

Score components	all queries	
	AR@1	AR@5
Object only	1.9 ± 0.5	8.2 ± 0.2
Object + part	2.4 ± 0.4	10.8 ± 0.9
Object + color	5.6 ± 0.5	15.5 ± 0.1
Object + attribute	8.5 ± 0.4	22.3 ± 0.2
Object + part + color	20.8 ± 0.6	40.2 ± 0.6
All	31.2 ± 0.4	52.2 ± 0.5

Table 18. Ablation study on importance of object, part, and attribute predictions on zero-shot instance detection performance. We compute metrics using only object, object + part, object + color, object + attribute, object + part + color, and all ViT-L FPN model scores.

ter. We report mean and standard deviation of results from that model over the same 4 query prompt variants as Detic.

I. Few-shot instance detection experiments

The few-shot model is a two-tower model as shown in Fig. 10, where the (a) first tower is a detection model which predicts object boxes in the images and (b) the second tower is an embedding model that provides a feature embedding for each of the predicted boxes. The two towers are learned independently.

Query feature registration. In the few-shot setup, for each query Q we are provided a set of “query images” with one bounding box per image for the “query” object instance. We first extract a feature for each of query boxes only using the

embedding model. Given k query images (with bounding box) for the query Q , we extract k query features. The features are then averaged to obtain an average query feature vector f_Q .

Instance detection with query features. We are also provided a set of target images for each query \mathcal{I}_Q from which another bounding box corresponding to the query needs to be extracted. For each image $I \in \mathcal{I}_Q$, we first predict 100 bounding boxes \mathcal{B}_I using the detection tower of our model. Each of these boxes $B \in \mathcal{B}_I$ are then represented by a feature vector $f_{B,I}$ using the embedding model. All the boxes are then ranked based on the cosine similarity of their feature with the query feature f_Q . The top N returned boxes from \mathcal{I}_Q are used to compute AR@N for $N = 1, 5$.

Detection model. We train a standard R50-FPN mask R-CNN model with 75 object categories on the train split of the PACO dataset. During the feature registration and instance detection stage, we ignore the category label and only use the predicted boxes.

Embedding model. The embedding model is a mask R-CNN style model with a custom ROI head as shown in Fig. 11. During inference, it takes predicted bounding boxes as input and outputs embeddings for each box with ROIAlign [18]. The model is trained with ArcFace [6] loss to have richer representations for instance recognition. We trained the embedding model with an ArcFace loss to perform 16464-way instance ID classification at box-level. The model was trained to distinguish the 16464 different object instances in the PACO-Ego4d train split. In this dataset,

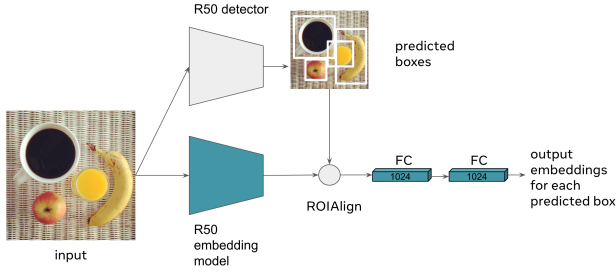


Figure 10. The few-shot instance detection model consists of a frozen detector and an embedding model. The detector outputs class-agnostic bounding boxes. The embedding model takes an image and a set of predicted bounding boxes on the image as inputs, and outputs embeddings for every box.

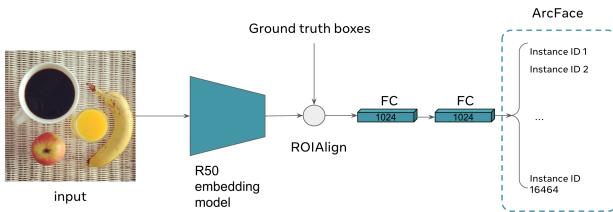


Figure 11. The embedding model is a mask R-CNN style model with a custom ROI head where the softmax loss is replaced with an ArcFace loss using instance IDs as supervision for richer representations for instance recognition. Once training is finished, we throw away the ArcFace layer and use the outputs from the last FC layer as per-box representations.

each instance has multiple bounding boxes, making it possible to train such a model. We simply use ground truth boxes during training to avoid handling the additional complexity from distinguishing foreground and background boxes. Note that the sets of instances in `train` and `test` splits are completely disjoint.

Implementation details. We use R50-FPN [31] as the backbone. The custom ROI head is implemented as a ROIAlign operator followed by 2 FC layers with 1024 dimensions. The ArcFace layer is configured with $margin = 0.5$ and $scale = 8.0$. We use the default data augmentation for Faster R-CNN [38] training in Detectron2 [47]. We train the embedding model on the PACO-Ego4D `train` split for 22.5K iterations. We set $lr = 0.04$ and use Cosine lr decay. The batch size is 128 distributed across 32 GPUs (4 images per GPU).

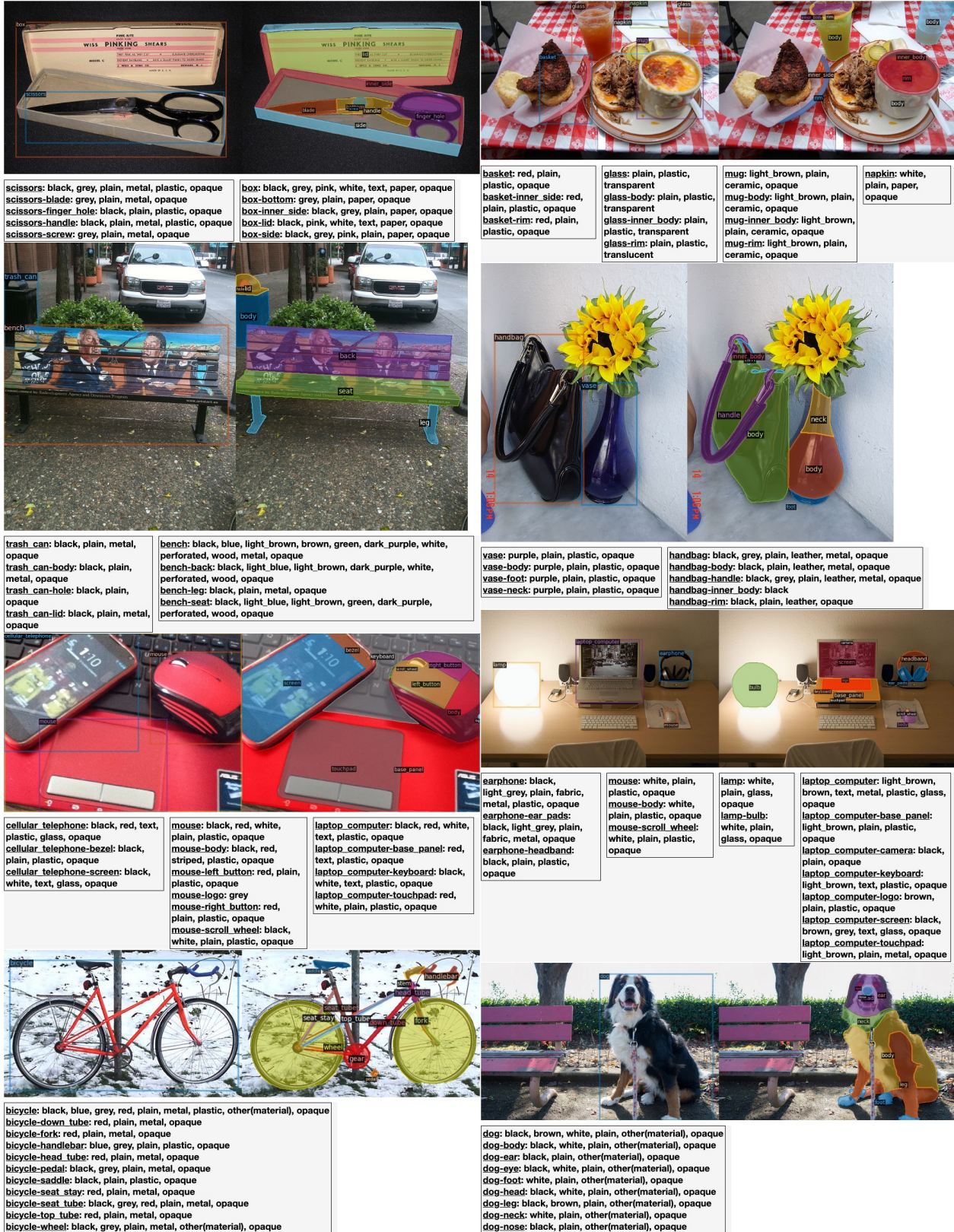
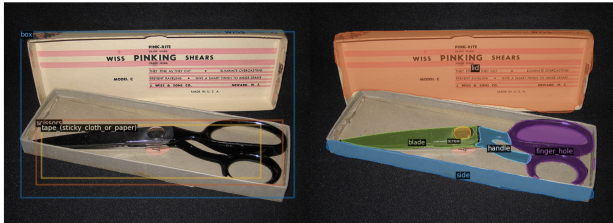


Figure 12. Annotation examples. Each image contains object bounding boxes (object masks omitted so attributes are visible) on the left and part masks on the right. Object and part attributes are listed below each image.



box:
opaque, black, white,
text, paper
box:lid: brown, green
paper, text, opaque
box:side: dark_grey
plain, opaque, grey,
paper

scissors:
opaque, black, grey, plain,
plastic
scissors:blade: black
metal, plain, opaque, grey
scissors:finger_hole: grey
plastic, plain, black, opaque
scissors:handle: dark_grey
plastic, plain, black, opaque
scissors:crew: dark_grey
metal, plain, opaque, grey

tape (sticky_cloth_or_paper): black, grey, plain,
metal, opaque



napkin: fabric, grey
plain, white, opaque

napkin: fabric, grey
plain, white, opaque

cup: light_grey, white, plain, plastic, transparent

cup:inner_body: brown, white, plain, plastic, transparent

cup:rim: brown, red, plain, plastic, transparent



bench: plain,
dark_green
wood, black, opaque
bench:back: brown,
text
wood, black, opaque
bench:leg: dark_grey
metal, plain, black,
opaque
bench:seat:
dark_brown, plain
wood, black, opaque

trash_can: plastic, dark_green
plain, black, opaque
trash_can:body: plastic, dark_green
plain, black, opaque
trash_can:bottom: black, dark_grey,
plain, metal, opaque

trash_can:lid: plastic, dark_grey
plain, black, opaque
trash_can:rim: black, dark_grey, plain,
plastic, opaque

car (automobile): white, black, plain,
metal, opaque

car (automobile):roof: white, grey, plain,
metal, opaque



vase: blue, dark_blue, glass
plain, opaque

vase:body: blue, dark_blue, glass
plain, opaque

vase:foot: black, dark_blue, ceramic
plain, opaque

vase:neck: blue, dark_blue, glass
plain, opaque

handbag: dark_purple
leather, plain, black, opaque

handbag:body: dark_grey
leather, plain, black, opaque

handbag:handle: dark_purple
leather, plain, black, opaque

handbag:rim: dark_brown
plain, leather, opaque, black



mouse (computer equipment): logo
plastic, red, black, opaque
mouse (computer equipment):body: logo
plastic, red, black, opaque
mouse (computer equipment):left_button:
light_pink
plastic, plain, opaque, red
mouse (computer equipment):logo:
opaque, light_grey, white, text, plastic

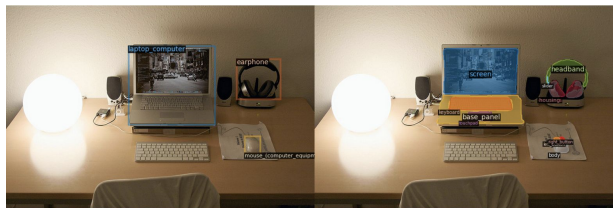
mouse (computer equipment):scroll_wheel:
light_grey, grey
plastic, plain, opaque

cellular_telephone: plain, white
black, opaque, glass
cellular_telephone:back_cover:
black, dark_grey, plain, plastic,
opaque

cellular_telephone:button:
black, grey, plain, plastic,
opaque

cellular_telephone:screen:
plain
white, black, opaque, glass

cellular_telephone: plain, white
black, opaque, glass
cellular_telephone:screen:
plain, light_blue
black, opaque, glass



laptop_computer: light_grey,
plain, grey
plastic, opaque

laptop_computer:base_panel:
light_grey, grey
plastic, plain, opaque

laptop_computer:keyboard:
light_grey, plain, grey
plastic, opaque

laptop_computer:screen: plain,
dark_grey
plastic, opaque, glass

laptop_computer:touchpad:
grey
light_brown, plain, metal,
opaque

earphone: grey
plastic, plain, black,
opaque

earphone:ear_pads:
plastic, grey
plain, black, opaque

earphone:headband:
dark_grey
plastic, plain, black,
opaque

earphone:housing:
black, grey, plain,
plastic, opaque

earphone:slider: black,
grey, plain, plastic,
opaque

mouse (computer equipment): grey
plastic, plain, white, opaque

mouse (computer equipment):body:
light_brown
plastic, plain, white, opaque

mouse (computer equipment):left_button:
white, light_grey, plain, plastic, opaque

mouse (computer equipment):right_button:
grey, light_grey, plain, plastic, opaque

Figure 13. Part segmentation and attribute prediction examples from a Vit-L model trained on PACO-LVIS and PACO-EGO4D. Each image contains predicted object bounding boxes for the 3 highest scoring objects on the left and predicted part masks which overlap with these objects on the right. The corresponding object and part attribute predictions are listed below each image. Attribute predictions in green are contained in ground truth.